Carbon 105 (2016) 52–76

Contents lists available at ScienceDirect

Carbon

journal homepage: www.elsevier.com/locate/carbon

Review article

The state of understanding of the lithium-ion-battery graphite solid electrolyte interphase (SEI) and its relationship to formation cycling☆

Seong Jin An [a, b], Jianlin Li [a], Claus Daniel [a, b], Debasish Mohanty [a], Shrikant Nagpure [a], David L. Wood III [a, b, *]

[a] Oak Ridge National Laboratory, Energy & Transportation Science Division, One Bethel Valley Road, P.O. Box 2008, Oak Ridge, TN 37831, USA
[b] University of Tennessee, Bredesen Center for Interdisciplinary Research and Graduate Education, 418 Greve Hall, 821 Volunteer Blvd., Knoxville, TN 37996, USA

ARTICLE INFO

Article history:
Received 10 December 2015
Received in revised form
31 March 2016
Accepted 4 April 2016
Available online 9 April 2016

ABSTRACT

An in-depth historical and current review is presented on the science of lithium-ion battery (LIB) solid electrolyte interphase (SEI) formation on the graphite anode, including structure, morphology, composition, electrochemistry, and formation mechanism. During initial LIB operation, the SEI layer forms on the graphite surfaces, the most common anode material. The SEI is essential to the long-term performance of LIBs, and it also has an impact on its initial capacity loss, self-discharge characteristics, rate capability, and safety. While the presence of the anode SEI is vital, it is difficult to control its formation and growth, as they depend on several factors. These factors include the type of graphite, electrolyte composition, electrochemical conditions, and temperature. Thus, SEI formation and electrochemical stability over long-term operation should be a primary topic of future investigation in the LIB development. This article covers the progression of knowledge regarding the SEI, from its discovery in 1979 to the current state of understanding, and covers differences in the chemical and structural makeup when cell materials and components are varied. It also discusses the relationship of the SEI layer to the LIB formation step, involving both electrolyte wetting and subsequent slow charge–discharge cycles to grow the SEI.

Contents

☆ Notice: This manuscript has been authored by UT-Battelle, LLC under Contract No. DE-AC05-00OR22725 with the U.S. Department of Energy. The United States Government retains and the publisher, by accepting the article for publication, acknowledges that the United States Government retains a non-exclusive, paid-up, irrevocable, world-wide license to publish or reproduce the published form of this manuscript, or allow others to do so, for United States Government purposes. The Department of Energy will provide public access to these results of federally sponsored research in accordance with the DOE Public Access Plan (http://energy.gov/downloads/doe-public-access-plan).

* Corresponding author. Oak Ridge National Laboratory, Energy & Transportation Science Division, NTRC-2, 2370 Cherahala Blvd., Knoxville, TN 37932-6479, USA.
E-mail address: wooddl@ornl.gov (D.L. Wood).

http://dx.doi.org/10.1016/j.carbon.2016.04.008

List of abbreviations

AFM	Atomic Force Microscopy
CL	caprolactam
CV	Cyclic Voltammetry
DEC	diethyl carbonate
DFT	Density functional theory
DMC	dimethyl carbonate
DMS	dimethyl sulfite
EC	ethylene carbonate
EDC	ethylene dicarbonate
EIS	Electrochemical Impedance Spectroscopy
EMC	ethyl methyl carbonate
EMI	1-ethyl-3-methylimidazolium
EV	electric vehicle
EVS	ethyl vinyl sulfone
FTIR	Fourier Transform Infrared Spectroscopy
GIC	graphite intercalated compound
HOMO	highest occupied molecular orbital
HOPG	highly oriented pyrolytic graphite
LC	Linear carbonate
Li	lithium
LIB	lithium-ion battery
LiBETI	Lithium bis(perfluoroethanesulfonyl)imide
LiBOB	Lithium bis(oxalato)borate
LiTFSI	Lithium bis(trifluoromethane sulfonyl) imide
LMR	lithium-manganese-rich
LUMO	lowest unoccupied molecular orbital
MC	Monte Carlo
MD	Molecular dynamic
MVS	metal vinyl sulfone
N/P ratio	negative electrode/positive electrode ratio
NMC	Li1+xNiyMnzCo1-x-y-zO2 or Nickel Manganese Cobalt oxide
NMR	Nuclear Magnetic Resonance
NR	Neutron Reflectometry
PC	propylene carbonate
PHEV	plug-in hybrid electrical vehicle
R-	alkyl group
SANS	Small-Angle Neutron Scattering
SEI	solid electrolyte interphase
SEM	Scanning Electron Microscopy
SIMS	Secondary Ion Mass Spectrometry
Sol	solvent
TEM	Transmission Electron Microscopy
TPD-MS	Temperature-Programed Desorption Mass Spectrometry
VC	vinylene carbonate
XPS	X-ray Photoelectron Spectroscopy
XRD	X-ray Diffraction

1. Introduction

Much effort has been put into lithium-ion battery (LIB) development for electric vehicles (EVs), plug-in hybrid electrical vehicles (PHEVs), and other electrical system applications [1–11]. Some of the key studies have involved reducing cost, increasing capacity retention, and improving efficiency [2,4–7,12–16]. During the operation of LIBs, a solid electrolyte interphase (SEI) layer (also called “solid electrolyte interface” in some literature) forms on the graphite surface, the most commonly used anode material, due to side reactions with the electrolyte solvent and salt. It is accepted that the SEI layer is essential to the performance of LIBs, and it has an impact on its initial capacity loss, self-discharge characteristics, cycle life, rate capability and safety. While the presence of the anode SEI layer is vital, it is difficult to control its formation and growth, as the chemical composition, morphology, and stability depend on several factors. These factors include the type of graphite, graphite morphology, electrolyte composition, electrochemical conditions, and cell temperature. Thus, SEI layer formation and electrochemical stability over long-term operation should be a primary topic of investigation in further development of LIB technology. This article reviews the state of knowledge on the formation process of the *graphite/carbon* SEI layer, its chemical composition, morphology, and associated reactions with the liquid electrolyte phase, and will address several important questions:

1.) Why is it important to understand the SEI layer composition and morphology, and how does it impact LIB performance (Sections 2–3)?
2.) What is the solid/liquid surface chemistry behavior at the nanoscale of the SEI layer (Sections 3–4)?
3.) What methods have been used to form the SEI layer during initial charging and discharging (Section 5)?

4.) What methods have been used to characterize the SEI layer properties such as composition, thickness, and morphology (Section 6)?
5.) What are the effects of different types of graphites and carbons on SEI layer properties (Section 7)?
6.) What are the electrolyte, binder, and conductive additive effects on SEI layer properties (Sections 8)?
7.) How is the SEI layer formation tied to the electrolyte wetting of the electrode (during cell manufacturing) and formation protocol, capacity fade, and cell lifetime (Section 9)?
8.) Why is it important to reduce the SEI formation protocol time during cell manufacturing (Sections 9–10)?
9.) How is the most recent understanding of the anode SEI layer impacting cell design and SEI durability (Section 11)?

This paper is a comprehensive review of the science of the LIB anode SEI layer and its relationship to electrolyte wetting, formation cycling, and cell lifetime. It spans from the basic science of the SEI formation interfacial physics and reaction mechanisms to the applied science of reducing formation cycle time and increasing LIB lifetime. The time period covered is from the discovery of lithium-ion intercalation in graphite (1979) up to the present day, and it offers insights into the SEI formation mechanism, chemical and morphological properties of the SEI, and relationship to formation cycling and cell lifetime. This paper will appeal to the entire LIB research community and the broader energy storage community as a whole. Given that it deals with an intricate combination of surface chemistry, electrochemistry, and reaction mechanisms, it will also appeal to chemists and chemical scientists in other fields.

2. Background

The anode SEI layer is formed from the so-called "lithium inventory" of the cathode and electrolyte salt, which is the total amount of lithium available for building the SEI and initial charging of the cell, and there is a delicate balance between the ideal surface area the anode should have and the energy and power density of an LIB. The entirety of the anode surface must have the SEI layer present to prevent further undesired decomposition of the electrolyte, which consumes Li ions. The amount of Li ion loss from the cathode directly affects the first-cycle irreversible capacity (energy density), while losing Li ions from the electrolyte lowers liquid-phase mass transport and increases electrolyte resistance thereby decreasing power density [1,17]. During the first full cycle, 10% of the original capacity is generally consumed in irreversible SEI formation [18]. Therefore, the total surface of the anode should be minimized from an energy density or cell cost standpoint. However, the minimization comes with a performance tradeoff – low anode surface area means lower power density (capacity at high C rates) with solid-state diffusion limitations. In contrast, high anode surface area is beneficial to power density, but much greater lithium inventory is consumed when passivating the surface to form the SEI layer, thereby decreasing energy density. Section 7 includes an overview and understanding of carbon/graphite properties and related SEI formation.

There is also a secondary connection of the SEI layer to LIB safety, and it comes into play once the anode is fully passivated. To avoid lithium plating or dendrite formation at the anode during charging over the life of the cell, capacity is often kept about 10% more than that at cathode [18] (N/P ratio of 1.1 where "N" is the negative electrode, or anode during cell discharging, and "P" is the positive electrode, or cathode during cell discharging) to prevent internal electrical shorts. Therefore, this extra anode material must also undergo SEI layer passivation adding to the cell cost and diminishing the total cell energy. Optimizing the N/P ratio is important for minimizing initial lithium inventory loss and decreasing initial irreversible capacity. For long-term capacity retention and Coulombic efficiency, optimizing only the capacity ratio would be insufficient because SEI continuously grows and consumes electrolytes and lithium ions when it is not well formed [19,20].

Better understanding of the state-of-the-art graphite SEI layer composition and morphology is an important step towards growing improved SEI layers that prevent continuous decomposition of electrolyte on the graphite surfaces. The anode SEI layer is composed of precipitates from reduced decomposition of solvents, salts, lithium ions, and impurities in the electrolyte due to their instability at the anode potential operating window [1,21]. It forms mostly during the first charge, but the formation continues slowly and gradually after first cycle until the SEI layer is fully developed, adding to the complexity of modern LIB formation protocols. An optimized SEI layer is expected to have negligible electrical conductivity and high electrolyte diffusion resistance while having high lithium ion selectivity and permeability. Once it is properly formed, further decomposition reactions with salts and solvents are prevented since electrons cannot transfer to or through the layer (the increased electronic resistance increases the potential on the graphite surface and shifts the surface potential to within the stability window of the electrolyte). However, in reality, the SEI layer gradually thickens during repeated charge–discharge cycles due to electron exposure to electrolyte or electrolyte diffusion to the graphite surface, although the layer thickness growth after a few charge–discharge cycles is not nearly as great as the amount during the first cycle. The gradual thickening of the layer further consumes Li ions, solvents, and salts and increases cell resistance. This continuous SEI layer growth during the formation cycling process lowers cell capacity and Coulombic efficiency.

It is worth mentioning briefly that a "SEI-like" layer forms on cathodes, as well, by oxidation reactions of electrolytes at high potentials [22,23], but its impact on cell performance is generally less. Recent studies involving lithium-manganese-rich (LMR) NMC materials ($Li_{1+x}Ni_yMn_zCo_{1-x-y-z}O_2$) for EV applications, show high capacities when operated at high voltage [3,14,24–28]. This cathode material has an operating window of 2–4.8 V vs Li/Li^+ and capacities of 200–250 mAh/g [24], but only 150 mAh/g within the typical operating voltage window (3–4.2 V) [15]. As the voltage approaches 4.7 V vs Li/Li^+ (or even less), decomposition takes place on cathode surface during charge or storage by oxidation of electrolyte solvent organic carbonates (ethylene carbonate, dimethyl carbonate ethyl methyl carbonate, propylene carbonate, etc.) [21,22,29,30]. Since these carbonates have oxidation (highest occupied molecular orbital (HOMO)) and reduction potentials (lowest unoccupied molecular orbital (LUMO)) around 4.7 V and 1 V vs Li/Li^+, respectively [21], they are decomposed by electro-reduction at the anode below 1 V and by electro-oxidation at the cathode above 4.7 V during charging or storage. The oxidation potentials of these carbonates are further reduced at elevated temperature (LIBs in vehicles or portable devices experience locally increased temperatures) to 4 V at 40 °C and 3.8 V at 60 °C [22,30–35]. Ethers and esters are not typically stable above 4 V [36,37]. Other species in the electrolyte, such as lithium compounds that are partially reduced at the anode and diffuse to the cathode, have even lower oxidation potentials. Wursig et al. reported SEI formation at 4.3 V vs Li/Li^+ and even at 25 °C on various cathode materials [38]. Hence, at high potentials, cathodes suffer from increases in resistance from SEI-like passivation layers as well as from loss or migration of active materials such as Mn and Co. When initial charge–discharge cycles and storage time are extended, the resistance at the cathode increases even more than that of the anode [39].

Despite the importance of understanding the formation, composition, morphology, and long-term structural and chemical evolution of the anode SEI layer, these topics are not yet fully understood because of analysis and measurement difficulties. In fact, the SEI layer formation mechanism is much less understood than the resultant chemical and physical properties themselves. The SEI is quite thin, a few hundreds of angstroms, and sensitive to moisture and oxygen in the air that may convert SEI components into different forms before or during analysis [40–42]. Because of the environmental sensitivity, SEI analysis requires inert and well-controlled conditions.

Functional properties for an ideal SEI layer are high electrical resistance and high lithium selectivity and permeability. Physical ones are a thickness close to a few Å, high strength, tolerance to expansion and contraction stresses (the SEI layer must accommodate expanding and contracting sub-surfaces during charging and discharging, respectively), insolubility in the electrolyte, and stability at a wide range of operating temperatures and potentials. Actual SEI layers seem to not yet have enough of these properties because it has been found that they keep growing over repeated charge–discharge cycles. This growth is closely related to lithium loss from both the electrolyte salt and cathode lithium inventory, as well as lithium diffusion resistance at the liquid interfacial zone adjacent to the SEI layer and within the SEI itself. The lithium consumption and diffusion resistance cause an increase not only in the overall cell resistance but also in anode potential. The increase in the anode potential is attributed to a lower number of Li ions in the electrode after consumption at the SEI. This increased anode potential also induces a similar increase in cathode potential to maintain a charge cutoff potential. When the cathode potential increases and reaches a certain point, the cathode crystal structure rearranges and distorts due to oxygen loss and transition metal shifting [3,14,24,25]. The electrolyte also becomes less stable at higher cathode potentials, which leads to solvent oxidation on the cathode surface (for example $LiPF_6$ in ethylene carbonate (EC): dimethyl carbonate (DMC)) is oxidized around 4.5 V vs Li/Li^+ during charging [43–47]. This gradual SEI growth on the anode negatively affects cathode potential and stability. Therefore, forming a robust and stable SEI layer on the anode carbon/graphite is essential for long LIB lifetime and high capacity retention.

SEI formation generally takes days because scan rates are slow, ~±C/5 down to ~±C/20 [13,15], to form a denser SEI structure rather than a highly porous one. After the first charge–discharge cycle, formation cycles generally repeat at different scan rates and/or different temperatures to build quality SEI layers. The longer the times and greater the number of charge–discharge cycles, the more expensive the process becomes, which also either lowers cell production rate or increases capital expense (i.e. more cycling stations required). If the electrical energy is not "recycled" (i.e. using the energy of one cell after charging it from the primary electricity source to charge another adjacent cell), the cost further increases. Reducing the time for SEI formation would provide higher production rates without needing extra space, equipment, and energy, eventually reducing battery pack and plant costs.

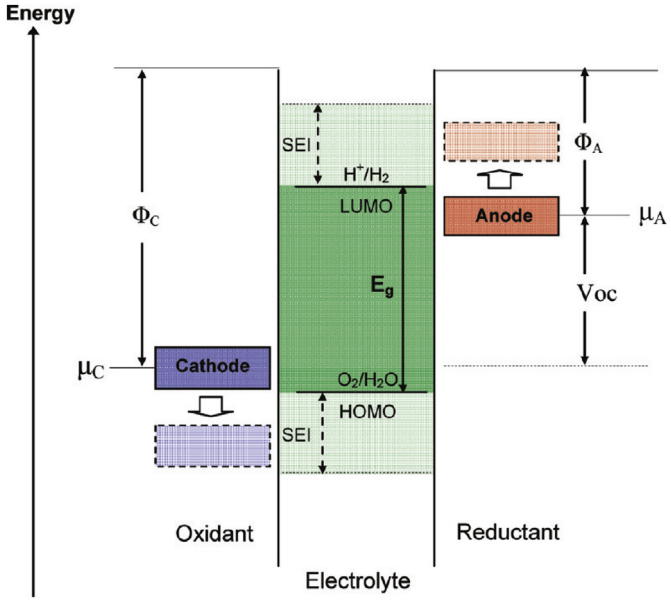

Fig. 1. Energetics of the formation of the anode and cathode SEI layers under electro-reduction and electro-oxidation conditions [21]. "Reprinted (adapted) with permission from (Goodenough, J. B.; Kim, Y. *Chemistry of Materials* 2010, 22, 587). Copyright (2010) American Chemical Society." (A colour version of this figure can be viewed online.)

3. Energetics of anode SEI formation

In LIBs an aprotic salt solution with low-molecular-weight organic solvents are the most widely used electrolytes. These electrolytes undergo decomposition at the graphite anode, and the SEI layer is formed from these decomposition products, which then dictates initial performance of the cell and long-term capacity fade characteristics. Therefore, the question is can the electrolyte decomposition be minimized or controlled to provide predictable performance of the cell.

Fig. 1 shows the relative electron energies of the anode, electrolyte, and cathode of a thermodynamically stable redox pair in a LIB. In the figure, μ_A and μ_C are the electrochemical potentials of the anode and cathode respectively. The stability window of the electrolyte is the difference between the energy of the LUMO and HOMO. This window is shown as E_g. If μ_A is above the LUMO energy, then it will reduce the electrolyte, and, likewise, if μ_C is below the HOMO energy, it will oxidize the electrolyte. The energy separation between the anode and cathode needs to be as high as possible to increase the energy density of the redox pair. The organic electrolytes used in LIBs have oxidation potentials around 4.7 V vs. Li^+/Li and reduction potentials close to 1.0 V vs. Li^+/Li. The intercalation potential of Li into graphite is between 0 V and 0.25 V vs. Li^+/Li, which is below the reduction potential of the electrolyte. Thus, the potential of the graphite electrodes falls below the stability window of the electrolyte during charging, and it decomposes at the graphite surface forming the SEI.

4. SEI features, morphology, and chemical composition

If all of the decomposition reaction potentials for the SEI formation are more positive than the anode Li ion intercalation potential, the SEI would form more completely under fast kinetics before the onset of the intercalation reaction. Once it is well formed, the SEI should have high Li-ion conductivity and negligible electronic conductivity. The electronically insulating property of the SEI prevents further reduction of the electrolyte on the graphite surface, while the ion conductive nature allows permeation of lithium ions to the graphite surface and provides pathways for the desired ion intercalation. To avoid cracking of SEI layers due to stress from a volume change of graphite during intercalation and de-intercalation and to avoid further passivation reactions, the molecular force between the SEI layer and graphite surface should be strong. Physically, the SEI layer should be strong or flexible enough to accommodate the volume change (expansion during charging and contraction during discharging) of the anode during the cycling process. Ideally, the SEI layer should be uniformly

distributed over the graphite surfaces. The chemical composition of the SEI should contain stable and insoluble compact inorganic compounds such as Li_2CO_3 rather than metastable organic compounds such as ROLi and $ROCO_2Li$ (where R is an low-molecular-weight alkyl group) [48,49], which is important for confining the loss of lithium inventory to the first few cycles and minimizing irreversible capacity loss. Insolubility of decomposed SEI components to an electrolyte is important for high capacity retention because loosing the components may induce new SEI formation where they dissolved out. According to MD simulations from Tasaki et al., the heat of salt dissolution in ED/DMC is in the order of $[CH_2OCO_2Li]_2$ (LiEDC, −22 kcal/mol) < $LiOCO_2CH_3$ (−4 kcal/mol) < LiOH < $LiOCO_2C_2H_5$ < $LiOCH_3$ < LiF < $[LiCO_2]_2$ < Li_2CO_3 (32 kcal/mol) < Li_2O (43 kcal/mol), indicating that inorganic Li_2O and Li_2CO_3 are endothermic and hard to dissolve in normal operation temperature while organic $[CH_2OCO_2Li]_2$ and $LiOCO_2CH_3$ are exothermic and the most soluble among the listed SEI components [50]. Inorganic products are hard to dissolve but can also diffuse into an electrolyte when surrounded by soluble organic products. Li_2CO_3 is generally abundant on a graphite anode than LiO_2 because of low concentration of lithium on surface of the graphite anode [51]. The concentration of LiO_2 can be increased on lithium metal anode.

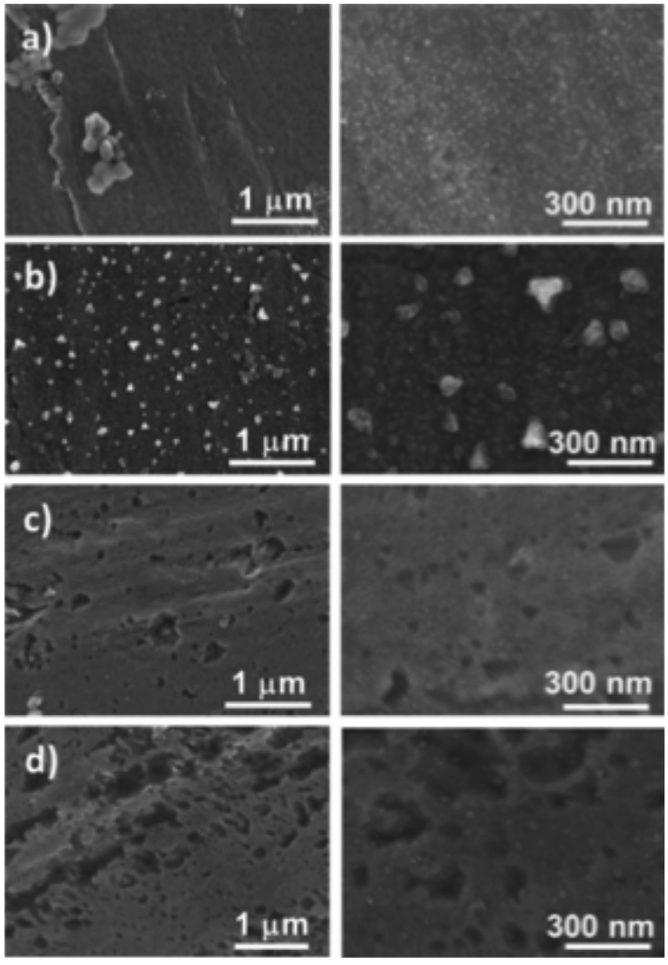

Fig. 2. SEI morphology at various formation potentials reported by Lu et al., (a) 0.7 V, (b) 0.5 V, (c) 0.3 V and (d) 0.0025 V. The right column images are higher magnification (100,000×) of the images in left column (30,000×) [56]. "Reprinted (adapted) with permission from (Harris, S. J.; Lu, P. *J. Phys. Chem. C* 2013, 117, 6481). Copyright (2013) American Chemical Society."

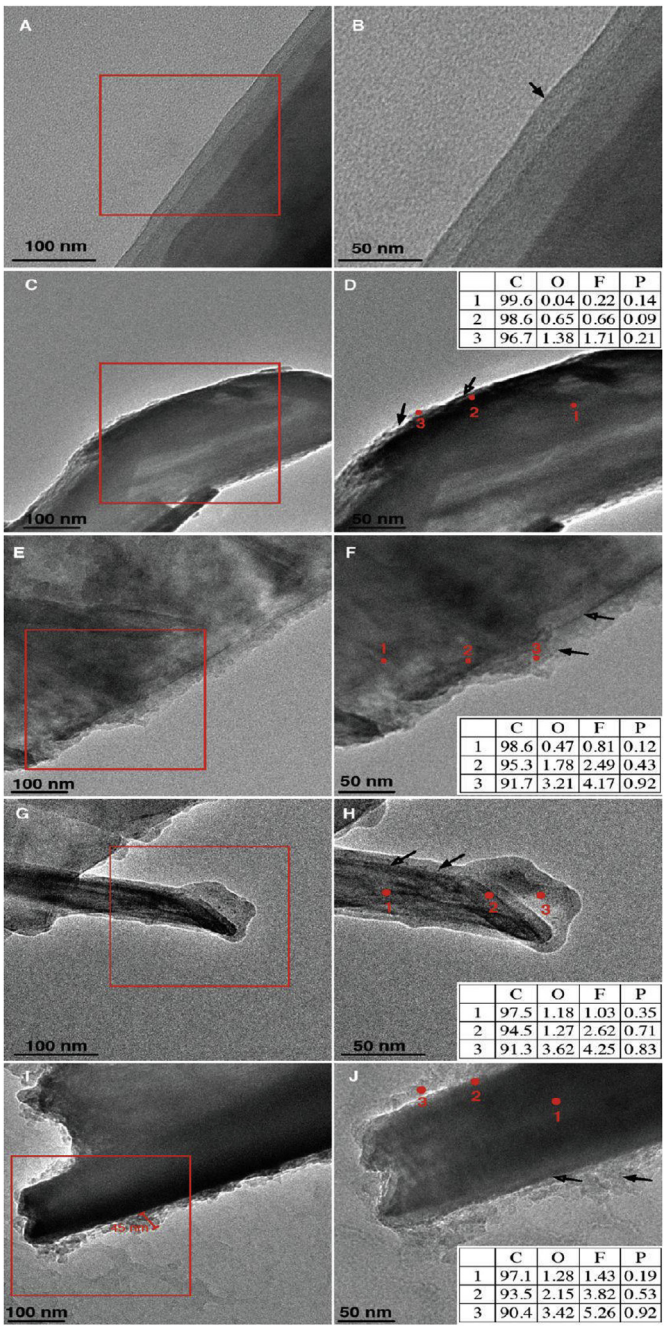

	C	O	F	P
1	99.6	0.04	0.22	0.14
2	98.6	0.65	0.66	0.09
3	96.7	1.38	1.71	0.21

	C	O	F	P
1	98.6	0.47	0.81	0.12
2	95.3	1.78	2.49	0.43
3	91.7	3.21	4.17	0.92

	C	O	F	P
1	97.5	1.18	1.03	0.35
2	94.5	1.27	2.62	0.71
3	91.3	3.62	4.25	0.83

	C	O	F	P
1	97.1	1.28	1.43	0.19
2	93.5	2.15	3.82	0.53
3	90.4	3.42	5.26	0.92

Fig. 3. TEM images of fresh graphite and SEI on graphite anodes cycled to four cutoff voltages in 1.2 M $LiPF_6$/EC during first charge reported by Lie et al., (A and B) Fresh graphite electrode, (C) 1.3, (E) 0.6, (G) 0.1, and (I) 0.05 V. The insets of (D), (F), (H), and (J) show element composition detected by EDX. The arrows indicate the SEI layer and the edge of graphite, and the red spots indicate locations probed by EDX [57]. "Reprinted with permission from (Mengyun Nie et al. *J. Phys. Chem. C*, 2013, *117* (3), 1257). Copyright (2013) American Chemical Society." (A colour version of this figure can be viewed online.)

From a historical standpoint, the SEI has been thought of as having a bilayer type structure. The layer near the interface of the electrolyte is assumed to be porous and less dense, composed of a large portion of organic components, and filled with electrolyte. This outer, organic layer may undergo further reduction, so its morphology may change in subsequent cycling. The inner layer adjacent to the graphite is presumed to consist mostly of inorganic compounds that protect the anode surface and prevent reduction.

Thus, it is assumed to have a denser morphology with lower porosity. In recent studies, the SEI structure shows a bilayer structure in general, but in reality is more complicated [51–54]. For example, according to the results of Takenaka's hybrid Monte Carlo (MC)/molecular dynamics (MD) reaction simulation, inorganic salts such as Li_2CO_3 are abundant near the anode surface and distributed within the whole SEI film, becoming Li_2CO_3 junctions for the organic lithium carbonates and stabilizing the SEI film [54]. Other recent computational studies have also shown detailed and complicated structures, even though they were based on many simplifying assumptions. Considering real-world LIB systems involving side reactions, impurities, and uneven current distribution, it is likely that SEI structures are even more complicated than those depicted by fundamental simulations.

Recently Lu et al. studied the morphological evolution of the SEI during the formation process [55,56]. Fig. 2 shows SEM micrographs at two different magnifications of the graphite anode surface from their study at different degrees of polarization during the first charge. The SEI thickness increased as the formation cycle proceeded (i.e. as the potential of the anode moved towards the intercalation potential). According to their model, the SEI at the beginning of the formation process contained mainly loosely held organic polymer compounds. As the potential was lowered, the SEI layer transformed into a more compact structure of inorganic salts. Figs. 2 and 3 captures this morphological evolution [55,57].

The SEI layer formed at the graphite basal plane differs in morphology and chemical composition from that formed at the edge plane. The SEI formed at the basal plane does not need to have ionic conductivity, but it does need to be electronically insulating and impermeable to other electrolyte components. Since lithium ions cannot intercalate into graphene layers across the basal planes, these planes are ionic insulators and do not contribute to reversible capacity. Hence, SEI formation at these locations should be minimized to avoid unnecessary loss of lithium inventory. Due to the different behavior of the SEI layer formed at basal and edge planes, the true SEI formation potentials are not captured by conventional electrochemical measurements.

The chemical composition and morphology of the SEI are affected not only by the electrolyte, but also by the chemical compositions and morphologies of carbon/graphite surfaces. In the case of the 1 M $LiPF_6$ in EC:DMC electrolyte and highly ordered graphite, the SEI at the edge plane is thought to be several times thicker (several nm) than that at basal plane. A thicker layer on the edge plane is consistent with the observation of higher reaction current at the edge plane than the basal plane [58]. On the edge sites for this particular case, the SEI is mainly composed of loosely packed inorganic lithium carbonates, organic lithium alkali carbonates and polymeric compounds on the electrolyte side. On the graphite side of the edge sites, the SEI is mainly composed of densely packed LiF, Li_2O, and Li_2CO_3. In between these two phases, there is an intermixed zone forming a trilayer structure. Overall, LiF and Li_2CO_3 make up more than half of the SEI layer [59,60]. On the basal sites, the SEI is composed of lithium carbonates more than LiF on the electrolyte side.

On the graphite side of the basal sites, the SEI is composed of similar portions of Li_2O, LiF, and lithium carbonates with small portions of polymeric compounds. LiF in the SEI is typically found in fluorine system electrolytes such as $LiAsF_6$, $LiPF_6$, and $LiBF_4$. Depending on LIB operating, anode sampling, and analysis conditions, the compositions of the SEI may vary even with the same electrolytes and electrodes used in a cell. $LiPF_6$ salts are unstable in elevated temperature and may precipitate into LiF during storage or operation. Lithium carbonates can be also decompose and form LiF after reacting with HF. Hence, LiF may be found in the SEI more frequently when there are other reactions before or during the surface analysis. HF formation, particularly observed in the case of $LiPF_6$ based electrolytes, is considered to dramatically affect the performance of LIBs by attacking the SEI layer. HF production during the SEI formation process is due to the reaction between decomposition products of the $LiPF_6$ salt and traces of water in the liquid electrolyte phase and/or adsorbed on the graphite surfaces. In recent studies, the amount of LiF found in the SEI still varies considerably from one study to the next. In particular, computational simulations rarely show LiF formation because they generally do not consider impurities like water causing HF production or self-decomposition from a salt, a poor assumption.

For the case of soft carbon in the same electrolyte, polymer and solvent reduction products are more prevalent than salt reduction products [61]. For other salts such as $LiBF_4$, LiTFSI, or LiBETI, the percentage of LiF is small and other carbonated species comprise most of the SEI layer [62]. In general, SEI layers are composed of densely packed inorganic compounds such as Li_2O, Li_2CO_3 and LiF on the graphite side and loosely packed inorganic and organic species like Li_2CO_3, lithium alkyl carbonate ($ROCO_2Li$) and polymer on the electrolyte side [63]. There are also other studies that argue large portions of inorganic Li compounds such as LiF are also found on electrolyte side [64–66]. These components, formed by solvent, lithium salt, and electrolyte additive decomposition, are neither uniformly distributed nor well-ordered within the SEI layer. These semi-quantitative concepts about SEI compositions are much less debated than those hypotheses with respect to exact composition, morphology, structure, and formation. The reasons for the uncertainty and inconsistency among different studies arise from analysis difficulty, different electrolyte compositions, different types of carbon/graphite, various SEI formation processes, and other physical and environmental conditions (i.e. temperature). Table 1 from Verma et al. provides a thorough list of the most agreed upon compounds found in the SEI on graphite anodes [48].

5. Formation mechanism of SEI layer

There are various reduction processes that compete with each other on the carbon/graphite surface during charging. The reactants are solvents, salts, additives, and trace air impurities (such as water). Electrochemical reaction rates differ depending on their intrinsic properties such as reductive potential, reduction activation energy, and exchange current density. They also depend on reaction sites (basal or edge), pre-decomposed precipitate sites, and many other different anode surface conditions [58,93–96].

Temperature, concentration of electrolyte salt, and reduction current rate significantly affect SEI formation as well [97]. When all of these variable conditions are mixed, it is difficult to analyze the SEI formation mechanism. However, it is generally accepted that $LiPF_6$ precipitates in the form of LiF or Li_xPF_y after reduction. Carbonates from the electrolyte solvent precipitate with lithium ions in form of Li_2CO_3, lithium alkyl carbonate ($ROCO_2Li$), or other organic compounds. While LiF, Li_2O, Li_2CO_3 and other insoluble products remain on the graphite surfaces as components of SEI layers, some soluble products from solvent decomposition may diffuse back into the electrolyte. Most reduction processes take place between 0.8 V and 0.2 V vs Li/Li^+ on highly ordered graphite. When the SEI is not fully developed, reduction continues below 0.2 V while lithium ions and solvent co-intercalate into the graphene planes. If this co-intercalation is excessive, the SEI layer may not fully develop because of continuous exfoliation. Fig. 4 illustrates these processes graphically.

In general it has been accepted that the SEI formation is a two-step process. During the first step when the graphite electrode is polarized, the components in the organic electrolyte undergo reductive decomposition to form new chemical species. In the

Table 1
List of known chemical compounds formed on the surface of carbon/graphite SEI layers ("Present" denotes that the compound was identified in the references given, and "Not Present" denotes that the compound was not identified) [48]. "Reprinted from *Electrochimica Acta*, 55, Verma P, Maire P, Novak, A review of the features and analysis of the solid electrolyte interphase in Li-ion batteries, 6332, Copyright (2010), with permission from Elsevier."

Component	Present	Not present	Notes
$(CH_2OCO_2Li)_2$	[66–69]		Being a two electron reduction product of EC; it is found mostly in the SEI formed in EC based electrolytes.
$ROCO_2Li$	[66,67,70,71]		They are present in the outer layer of the SEI. They occur in most PC containing electrolytes, especially when the concentration of PC in the electrolyte is high.
Li_2CO_3	[67,68,71,72]	[70,73–75]	It may also appear as a reaction product of semicarbonates with HF, water, or CO_2.
ROLi	[73,75–78]		Most commonly found in the SEI formed in ether electrolytes like tetrahydrofuran (THF), but may also appear as DMC or ethyl methyl carbonate (EMC) reduction product [72]. It is soluble and may undergo further reactions [79].
LiF	[72,74,80]		Mostly found in electrolytes comprising of fluorinated salts like $LiAsF_6$, $LiPF_6$, $LiBF_4$. It is a major salt reduction product. HF contaminant also reacts with semicarbonates to give LiF byproduct. Amount of LiF increases during storage [74].
Li_2O	[74,81,82]	[80,83–85]	It may be a degradation product of Li_2CO_3 during Ar+ sputtering in the XPS experiment.
Polycarbonate	[80,86]		Present in the outermost layer of the SEI, close to the electrolyte phase. This part imparts flexibility to the SEI.
LiOH	[69,87,88]	[80,81]	It is mainly formed due to water contamination [89,90]. It may also result from reaction of Li2O with water or with aging [75].
$Li_2C_2O_4$	[75,78]		It is found to be present in 18,650 cells assembled in Argonne National Laboratory containing 1.2 M $LiPF_6$ in EC:EMC (3:7) electrolyte. Li carboxylate and Li methoxide were also found in their SEI [75].
HF	[91,92]		It is formed from decomposition $LiPF_6$ and the water in the solvents. It is highly toxic and can attack components of the cell.

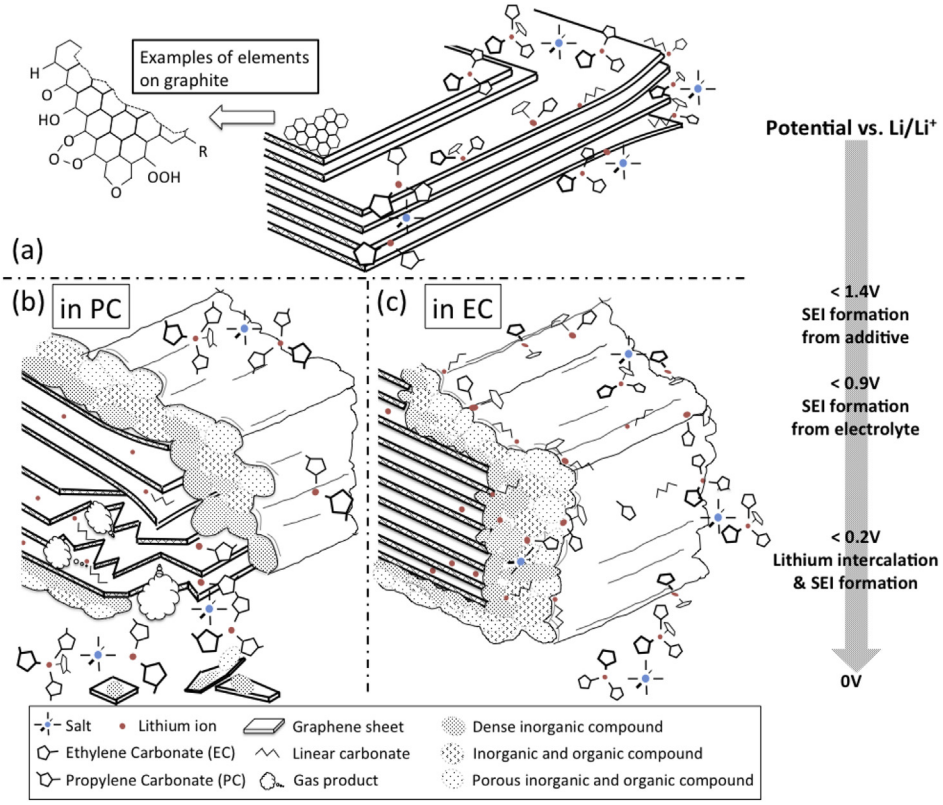

Fig. 4. Schematic of the anode SEI formation process showing (a) graphene layers surrounded by electrolyte salts and solvents above 1.4 V vs. Li/Li^+, (b) propylene-carbonate (PC) intercalation with lithium ions into graphene layers resulting exfoliations below 0.9 V vs. Li/Li^+ and (c) stable SEI formation in ethylene-carbonate (EC)-based electrolyte below 0.9 V vs. Li/Li^+; plane side with thinner SEI and edge side with thicker SEI. (A colour version of this figure can be viewed online.)

second step, these decomposition products undergo a precipitation process and begin forming the SEI layer until all the sites on the graphite surface are covered. Even though several studies have been conducted to understand the formation mechanism of the SEI, it has been a major topic of debate, which centers on the reduction pathways, especially of the solvent molecules. There are typically four different reactions possible during the first cathodic polarization of the graphite electrode. The pathways of the four reactions are shown schematically in Fig. 5.

The ionic radius of a Li ion (0.59 Å) [99] is much smaller than the corresponding anionic counter ion in the salt. Due to this size difference, Li ions are strongly solvated in the electrolyte solution, which also contains weakly solvated anions (such as PF_6^-) and isolated solvent molecules [100]. The solvated Li ions diffuse towards the surface of the graphite electrode due to the concentration polarization in the liquid phase. At the graphite surface, these solvated ions can undertake different pathways leading to different reductive decomposition products.

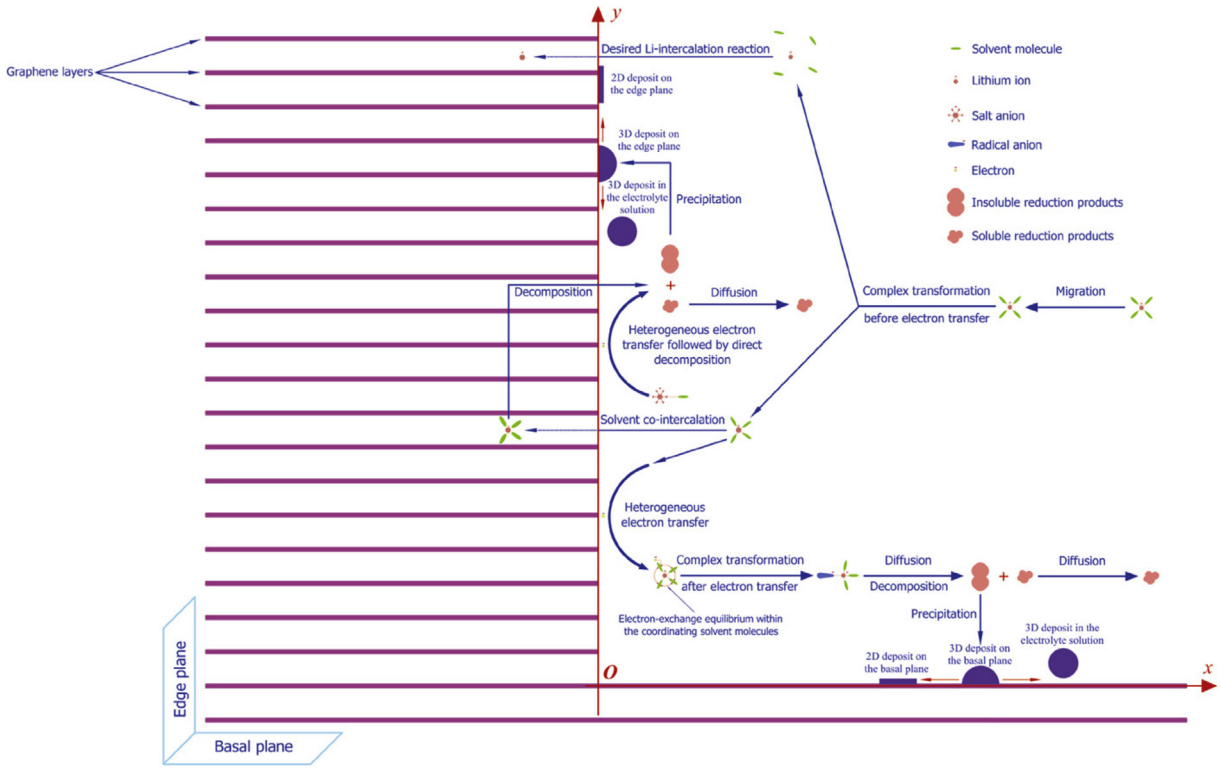

Fig. 5. Proposed SEI layer reaction mechanism consisting of a four-step pathway (Yan) [98]. "Reprinted from *Electrochimica Acta*, 55, Jian Yan, Jian Zhang, Yu-Chang Su, Xi-Gui Zhang, Bao-Jia Xia, A Novel Perspective on the Formation of the Solid Electrolyte Interphase on the Graphite Electrode for Lithium-Ion Batteries, 1788, Copyright (2010), with permission from Elsevier." (A colour version of this figure can be viewed online.)

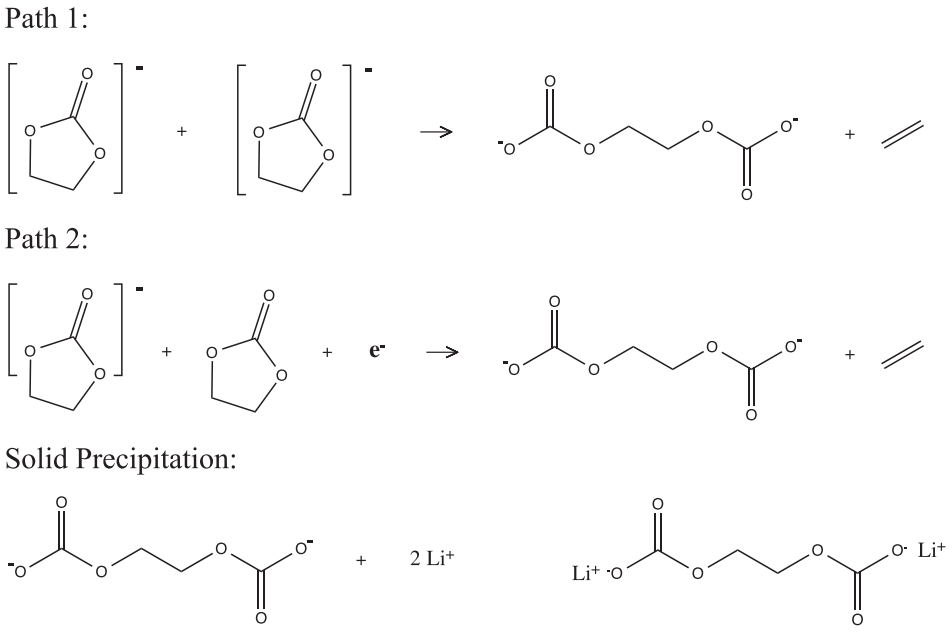

Fig. 6. Decomposition and precipitation pathways of ethylene carbonate anion.

i. Intercalation of Li ion without the solvation shell into the graphene layers.
ii. Heterogeneous transfer of electrons from the solid phase graphite electrode to the solvent molecules.
iii. Co-intercalation of the solvent molecules with the solvated Li ions into the graphene layers.
iv. Heterogeneous transfer of electrons from the solid phase graphite electrode to the salt anions.

These possible pathways are based on electron transfer to salts/solvents in electrolyte solutions caused by the cathodic polarization of the electrode, thermodynamic simulations using molecular

orbital calculations, and ionic sizes. Among these possibilities, reaction (i) is the desired reaction and leads to the faradaic current within the cell. This reaction occurs at a potential more negative than the potential of the other reactions, so during cathodic polarization, other reactions are preferred until the potential drops close to the intercalation potential. Reactions (ii) and (iii), which address the reduction of the solvent molecules, are the major source of debate in the literature. According to Dahn and Aurbach, the reduction of a solvent molecule (for example [EC]-) is a one-electron reaction occurring at the surface of the graphite. Therefore, according to this hypothesis, reaction (ii) proceeds with the solvent molecule being reduced to form an intermediate radical anion. This radical anion undergoes further decomposition according to one of the pathways shown at Path 1 or 2 in Fig. 6, and finally solid lithium ethylene dicarbonate (LiEDC) precipitates as shown below the Path 2. Aurbach [49,79] also argued that LiEDC is extremely reactive with traces of water in the electrolyte and forms Li_2CO_3 upon reacting.

According to the second theory proposed by Dey et al. [101], Besenhard et al. [102] and Chung et al. [103], reaction (iii) is a more preferred reaction and [EC-] undergoes a two-electron reduction reaction. The solvated Li ions are co-intercalated into the graphene layers held by weak van der Waals forces and form intermediate ternary graphite intercalated compounds (GIC) such as $[Li(Sol)_xC_y]$. The ternary GICs are subsequently reduced to form the SEI. Since the literature supports both hypotheses, the proposed mechanisms are still debated. Reaction (ii) and reaction (iii) may even compete against each other and both might occur in parallel during the SEI formation process. Reaction (iv) is the heterogeneous transfer of electrons directly to the salt anions to form inorganic SEI products.

6. Methods of analyzing and characterizing the SEI layer

SEI layers easily react with ambient CO_2 and H_2O to form inorganic lithium-containing compounds such as Li_2CO_3 and Li_2O [42,89,104]. Hence, washing the electrode in electrolyte solvents for analysis can easily introduce artifacts in the morphology and chemical composition of the SEI layer. For example, $ROCO_2Li$ and ROLi react with CO_2 to form Li_2CO_3 [105]. The lithium in the SEI will also react spontaneously with atmospheric oxygen to form various lithium oxides (Li_2O, Li_2O_2 and LiO_2) [36]. These oxides are strong nucleophiles and react further with organic solvents and semi-carbonates to form carbonates and alkoxides [106]. Thus, specialized sample chambers are necessary when transferring SEI specimens from the inert atmosphere of a glove box to an analytical instrument to avoid chemical contamination and physical damage.

A variety of tools and techniques have been used to analyze the SEI, including traditional electrochemical methods such as electrochemical impedance spectroscopy (EIS) and Cyclic Voltammetry (CV). EIS is a nondestructive analysis tool, which provides useful information from a complex electrochemical system having a diffusion layer, electrolyte resistance, electrode kinetics, and double-layer capacitance [55,64,107–114]. To diagnose EIS spectra properly, a good equivalent circuit model is required. CV, which measures current in the anodic (oxidation) and cathodic (reduction) directions, has also been successfully implemented to understand the SEI [112,114–119]. Traditional tools of scanning electron microscopy (SEM) [38,55,64,112,116,120–123], transmission electron microscopy (TEM) [65,118,121,124,125], scanning tunneling microscopy (STM) [119,126], atomic force microscopy (AFM) [64,85,126], and Ellipsometry [115] have been implemented to image the surface features and morphology of the SEI. TEM can also show surface crystallinity, in-situ interface formation, and lithiation/delithiation in operando [127–129]. AFM is a useful tool for studying SEI morphology and thickness because it can measure differences in depth at Angstrom resolution. Ellipsometry is a non-destructive optical tool that measures thickness and roughness of thin films by using reflectance ratios, but its weakness is that the measured signal depends not only on thickness, but also material properties.

Because the anode SEI is a thin layer on graphite, surface analysis tools such as X-ray photoelectron spectroscopy (XPS) [16,55,62,64,65,91,110,112,116,118,121,123,124] and Fourier transform infrared spectroscopy (FTIR) [64,118,125,126] have been used for characterization because of their surface sensitivity and chemical identification ability. Raman spectroscopy [16,64,121], X-ray diffraction (XRD) [16,121], Secondary Ion Mass Spectrometry (SIMS) [55,65], nuclear magnetic resonance (NMR) [92,109,110,118], neutron reflectometry (NR) [130], small-angle neutron scattering (SANS) [131], and temperature-programed desorption mass spectrometry (TPD-MS) [120] have also been successfully applied to identify SEI surface species.

7. Effects of carbon/graphite properties on SEI formation

Carbons are widely used as LIB anodes because of their stability and low working potential. Graphite is a crystallite and the most stable allotrope of carbon. It has perfect stacking of graphene layers in AB form and in some cases ABC form. In general, aggregates of perfectly stacked graphite crystallites exist with different orientations in an electrode. Graphite has a redox potential very close to Li/Li^+, is safe, is the most stable form of carbon, is environmentally benign, and has low (pre-processed) cost. A lithium atom is intercalated between the graphite layers to form an intercalation compound (i.e. LiC_6) during LIB operation [19,20]. The intercalation reaction prevents the deposition of metallic lithium on the graphite surface and avoids dendritic growth making these types of LIBs safe. The lithium-ion charge is also maintained, essentially eliminating the activation energy associated with the formation of a chemical bond. The carbon is reduced to maintain charge balance.

Fig. 7 shows an aggregate graphite particle and the graphite layers within that particle. In a crystallite of graphite, the two characteristic surfaces are referred to as basal and edge planes. The surfaces parallel to the graphene layers are called basal planes, and the surfaces normal to the graphene layers are edge planes. Lithium predominantly intercalates into the graphene layers through the edge planes in the direction parallel to the basal plane. The SEI formation process also differs at these two planes. Thus the ratio of basal plane to edge planes determines electrochemical performance of graphite electrodes. Different types of graphite such as highly oriented pyrolytic graphite (HOPG) and natural graphite have been used as anodes. Since the basal plane to edge plane ratios will differ in different forms of graphite, the SEI formation process will be different, as well as the chemical and physical properties of the SEI layer. In turn, these property differences will affect electrode performance during early life and the shape of the long-term capacity fade curve.

The SEI layer forms differently depending on composition and structure of carbon/graphite surface. The key factors for SEI formation are particle size, basal-to-edge-plane ratio, pore size, degree of crystallinity, and surface chemical composition (adsorbed species) [132,133]. The surface area of small particles is greater than that of large ones for the same weight. Smaller particle size generally causes more edge sites, as well as more SEI formation surface area. The decomposition on basal planes and edges differs because edge sites provide better reactivity than basal ones. Hence, electrolyte decomposition occurs at edge sites first. The edge sites are also the access points for lithium intercalation to graphene layers. Lithium ions diffuse along with solvent molecules and salts. At a potential lower than 0.2 V vs. Li/Li^+, lithium intercalation into

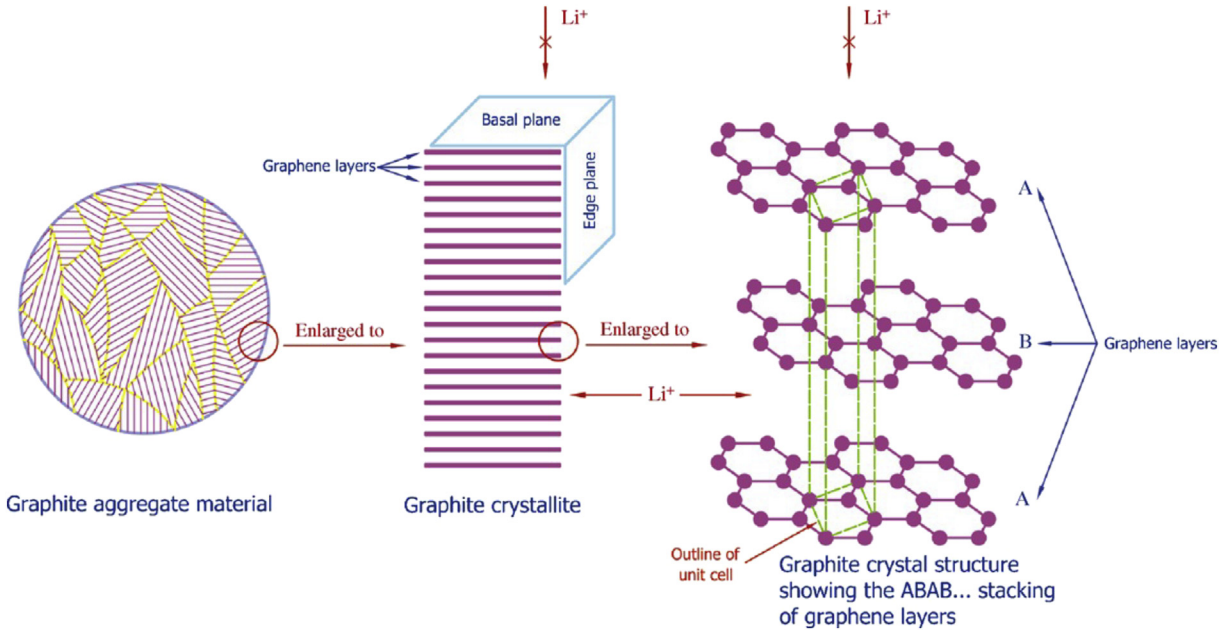

Fig. 7. Schematic of the lithium-ion intercalation process into and out of graphite [J. Yan et al.] [98] Left: graphite particle showing turbostratic disorder of individual nano-scale regions of high order (crystallinity). Center: graphene layers of an individual crystallite showing edge and basal plane directions. Right: AB stacking of individual graphene layers where lithium ions intercalate between layers A and B. "Reprinted from *Electrochimica Acta*, 55, Jian Yan, Jian Zhang, Yu-Chang Su, Xi-Gui Zhang, Bao-Jia Xia, A Review of the State of Understanding of the Graphite Solid Electrolyte Interphase (SEI) and Its Relationship to Formation Cycling, 1787, Copyright (2010), with permission from Elsevier." (A colour version of this figure can be viewed online.)

the graphene layers via edge sites begins. This intercalation generates concentration differences inducing solvent and salt reactants to move towards the edge sites and decompose there if the edge sites are not fully occupied by the SEI layer. This process also results in a thicker SEI on edge sites than on basal planes.

Few studies have been reported on the effect of the graphite particle size distribution, porosity, surface roughness, surface chemistry and crystallinity [120,132,134–137]. Graphite with low specific surface area tends to exfoliate more. As the surface area is decreased by heat treatment, the number of surface defects increases and the exfoliation tendency of the graphite further increases. Above a critical specific surface area of 0.2 m^2/g, the exfoliation tendency is suppressed in the absence of surface defects [120]. Graphite particle sizes with surface areas of 1–5 m^2/g may mitigate exfoliation without introducing excessive irreversible capacity loss. The degree of graphite crystallinity is also an important factor in SEI formation, and highly ordered graphite is preferred for high-energy LIB anodes. When the particle size is small, irreversible capacity loss increases due to larger surface area for lithium inventory loss during SEI formation (a side benefit, though, is that the power density increases with smaller anode particle size). Increasing graphite size is one way for lower irreversible capacity loss and higher energy density, but large particle sizes increase the probability of exfoliation.

Chemical composition on carbon/graphite surfaces may also affect the exchange current density and potential for SEI formation, as well as wettability of electrolyte, chemical adhesion between carbon and the SEI layer after decomposition, and between carbon and electrolyte before decomposition [64,93,138–144]. The presence of oxygen species on graphite surfaces increases the reduction potential vs Li/Li^+ and helps early SEI formation before lithium intercalation. The presence of these species has been shown to be vital in SEI formation by serving as nucleation sites for electrolyte decomposition, and a lack of them can hinder the decomposition reactions and increase the exfoliation of the graphene layers [145]. Oxygen species on graphite surfaces can be attached by heat treatment in various environments. Natural graphite usually has oxygen-containing species on its surface, although the degree of crystallinity may not be that high. To increase it, calcination in air produces more crystallites and increases the adsorbed oxygen-containing species.

8. Effects of electrolyte composition on SEI formation

LIB liquid electrolytes are commonly composed of a combination of low-molecular-weight organic solvents like ethylene carbonate (EC), dimethyl carbonate (DMC), diethyl carbonate (DEC), ethyl methyl carbonate (EMC), or propylene carbonate (PC) and lithium salts like $LiPF_6$ or $LiBF_4$. Because of the high oxidation potential (4.7 V vs. Li/Li^+) of these organic carbonates, SEI formation is prevented on the cathode surface during charging. PC had historically been a widely used solvent because it is a liquid at cell operating temperatures and has a high dielectric constant ($\varepsilon = 64$) [146]. The dielectric constant is an important indicator that predicts degree of salt dissolution. The drawback of using PC is severe solvent co-intercalation with lithium ions into graphite that exfoliates the graphene sheets, forming decomposition products within the sheets and releasing gases like propylene. Instead, EC is widely used because of its high dielectric constant ($\varepsilon = 89$) and stable SEI formation, although its high viscosity and melting point of 36 °C require thinning solvents such as DMC, DEC, and EMC. For example, 1–1.2 M $LiPF_6$ in 1:1 wt ratio of EC/DEC is a common electrolyte composition. In mixtures of EC/DEC or EC/DMC, $LiPF_6$ dissolves well and yields ionic conductivities of up to ~10^{-2} S/cm^{-1}, a high reduction potential of 1.3 V vs Li/Li^+, and an oxidation potential of above 4.5 V vs Li/Li^+. This combination results in excellent electrolyte properties, but it is highly flammable.

$LiClO_4$ has high ionic conductivity (5.6 mS/cm in PC, 8.4 mS/cm in EC/DMC) and may form less resistive SEI layers than $LiPF_6$ and $LiBF_4$ due to no LiF decomposition. The drawback is thermal

instability that the salt reacts with solvents at elevated temperature and it is explosive. $LiBF_4$ shows better thermal stability and less sensitivity to moisture than $LiPF_6$. But it was not commonly adopted in industry because of low ion conductivity (3.4 mS/cm in PC, 4.9 mS/cm in EC/DMC): about 40% lower than $LiPF_6$ (5.8 mS/cm in PC, 10.7 mS/cm in EC/DMC) and high resistance of SEI from $LiBF_4$ electrolyte [147]. Lithium Bis(trifluoromethanesulfonyl) imide(Li Imide) is highly ion-conductive (5.1 mS/cm in PC, 9.0 mS/cm in EC/DMC) and thermally stable: no decomposition until 360 °C. But it has a serious Al corrosion issue. $LiAsF_6$ is not adopted in industries because of concerns about the toxicity of As(V) although it has high ion conductivity. $LiPF_6$ is a well-known salt that is currently used in industries. It may not be the best in all requirements for an electrolyte but well balanced. In terms of safety, an inorganic electrolyte of $LiBF_4$ in 1-ethyl-3-methylimidazolium tetrafluoroborate (EMI-BF_4) is one alternative due to its higher boiling point than $LiPF_6$ in EC/DEC and non-flammability. EMI-BF_4 also has a higher oxidation potential, but its ionic conductivity is lower due to the high solvent viscosity. Lithium bis(oxalato)borate (LiBOB) also has less thermal reactivity. It is used as a salt by itself or an additive in an electrolyte. LiBOB stabilizes the graphite structure effectively even in pure propylene carbonate (PC) and facilitates SEI formation on the surface of electrode materials. On the other hand, its solubility and conductivity in other common solvents such as EC and PC are inferior. However, these limitations are improved by using a more appropriate solvent such as dimethyl sulfite (DMS) with γ-butyrolactone (γBL) [148,149].

In order to enhance early and stable SEI formation on the graphite anode surface and to prevent exfoliation during the lithium intercalation, liquid additives are often used in organic electrolytes. The most commonly used additive is vinylene carbonate (VC), and it has lower reductive activation energy (13 kcal/mol) and higher reduction potential (1.05–1.4 V Li/Li^+) than EC (24.9 kcal/mol and 0.65–0.9 V Li/Li^+, respectively) and PC (26.4 kcal/mol and 0.5–0.75 V Li/Li^+) [36,150,151]. VC added to PC promotes reductive decomposition at potentials around 1.3 V. About 3 wt% of VC is usually incorporated and improves cycle life and Coulombic efficiency by creating a more stable SEI layer. During the first charging step, VC in EC or PC increases the reduction potential by around 0.2 V, so the solvent mixture decomposes earlier in the formation process than without VC, which starts building an enhanced SEI layer before lithium intercalation begins. When VC is used in EC, it is possible to have large portions of polymer species in SEI [152].

Tasaki et al. investigated the reduction activation energy of various additives in the presence of a lithium anode [150]. This study showed that reduction activation energy (energy difference between the reactant and its transition state) of VC is 13 kcal/mol, which is lower than that of EC (24.9 kcal/mol) and PC (26.4 kcal/mol) and indicates the tendency of VC to reduce easier than EC or PC. Regarding reduction potential, Yoon et al. [153] reported reduction potentials of various additives including VC and N-substituted caprolactam (CL) derivatives. The reductions of CL, VC, and EC take place at 1.10 V, 1.05 V, and 0.65 V vs. Li/Li^+, respectively. Jung et al. [154] also obtained similar results via DFT calculations and experiment and showed that EC (0.6 V vs. Li/Li^+, −55.9 kJ/mol Gibbs free energy of reduction) has lower reduction potential than VC (0.75 V vs. Li/Li^+, −160.0 kJ/mol Gibbs free energy of reduction), which agrees with the calculations of Tasaki et al. On the other hand, Wang et al. [155,156] found different results from a polarized continuum model in calculating reduction activation energy of $(EC)_nLi^+(VC)$, n = 1–3. Ring-opening barriers of EC (8.8–11.1 kcal/mol) were found to be lower than that of VC (20.1–21.1 kcal/mol) for reduction reactions, and a major conclusion was that EC decomposes more readily than VC because VC acts as a stable anion intermediate and assists nearby EC reduction. Although the calculations from Wang et al. [156] yielded slightly different results, agreement was found that VC increases solvent reduction reaction rates. Considering reduction potential, reaction enthalpy and activation energy, VC is reduced before EC and PC do during a reduction cycle (charge) although the reduction products of VC may not be as stable as those of EC and PC [153]. In industry, many different proprietary additives are used in even more combinations together with variations on the formation protocol, and the resulting SEI structures are closely guarded.

9. Relationship between electrolyte decomposition reactions and LIB formation protocol

In 1979, Peled first used the term solid electrolyte interphase (SEI) for the LIB anode passivation layer [140], and, in 1990, Dahn et al. discovered the advantage of using EC in the electrolyte for forming the SEI [157]. Before the use of EC was commonplace, PC was the most widely used LIB electrolyte solvent, which was highly compatible with lithium metal anodes. Early LIBs implemented lithium anodes, but dendrite growth was a problem in terms of safety and long-term performance [158–161]. Once the discovery of graphite as a safe, high-performing anode intercalation material was made, its major drawback was also quickly discovered. PC easily co-intercalates with lithium ions and exfoliates the graphene layers during electrolyte decomposition, while also releasing propylene gas. Attention shifted to using amorphous carbons having little crystallinity because they tended to exfoliate much less in PC based electrolyte solutions and showed good reversible capacity. The problem with these materials, though, was high initial capacity loss due to thick SEI layer formation. When Dahn et al. found that EC reduced the first-cycle capacity loss (due to a much thinner SEI layer formation) and increased the stability of the SEI by mitigating exfoliation of graphite, solvent mixtures high in EC concentration were mainly used. As the appreciation of having a stable, durable SEI has grown since the early 1990s, much effort has been dedicated to: 1) improving its formation by using additives that result in better SEI-layer architectures; 2) modifying the anode surface for improving exchange current density and charge–discharge reaction kinetics; 3) implementing charge–discharge cycles that enhance layer formation; and 4) developing alternative electrolytes that result in less lithium inventory loss during formation.

Current densities, cut-off voltages, and temperatures used during formation cycling have all been shown to have a profound effect on the chemical and microstructural properties of the SEI layer. It starts to form around 0.8 V vs Li/Li^+, and the thickness gradually increases until around 0.3 V vs Li/Li^+. At higher charging anode potentials vs Li/Li^+, the SEI is composed of loosely aggregated organic components with lower ionic conductivity. As the anode potential drops, the SEI becomes more compact and begins to contain inorganic components with higher conductivity. The kinetics of the different SEI forming reactions can be exploited by varying the current densities and temperature. At higher current densities, the formed SEI has a more porous nature with high electronic and ionic conductivity. At lower current densities, the formed SEI is denser with lower electronic conductivity and higher ionic conductivity, which is the main reason formation protocols have historically required extremely low first-charge (and even low second and third charge) rates [121,162,163]. Elevated temperature also enables formation of a stable SEI.

Few studies have been reported on electrolyte wetting of electrodes, although it is an important factor for reducing SEI formation time and manufacturing resources that directly affect LIB pack cost. In fact, wetting takes the majority of cell production time and involves many of the latter manufacturing steps such as addition of

insulators, seals, and safety devices [7]. It takes many hours for electrolyte to completely wet the separator and reach the smallest pores of the electrodes [15], and studying wetting transport phenomena without a complete cell assembly facility is difficult.

Wetting electrodes (at low vacuum pressures during electrolyte filling and subsequently at elevated temperature after cell sealing) with electrolyte and forming SEI layers requires ~0.5–2 weeks for the entire process [7,15]. Wood et al. reported costs for a general wetting and formation process, which showed the SEI formation can contribute up to $32–33/kWh of usable energy for the battery pack cost (out of a total cost of ~$500/kWh) [15]. Anode and cathode electrodes need to be fully wetted with electrolyte during the initial portion of formation cycling, which is the process of the first 1–2 successive, slow and shallow charge–discharge cycles of a cell's life where the anode SEI layer is first formed. The initial wetting process is slow because the electrolyte has to permeate into all pores of the separator and electrodes in a near fully assembled cell. Evacuating gases out of the pores under high vacuum during cell assembly can accelerate infusion of the electrolyte and enable uniform distribution, although it requires more equipment and processing expense. Even under an evacuated condition, the smallest pores of the electrodes and separator may not fully wet unless they have a higher surface energy than the electrolyte. This situation is due to the competition between hydrodynamic forces at low pressure and non-wetting surface forces (the smaller the pore size, the lower the vacuum pressure needed to make a non-wetting liquid enter a pore). To avoid costly and time-consuming vacuum pumping, both electrodes (and the separator) should have high wettability of the electrolyte for full active material utilization during the formation cycling process. The formation process cannot commence until full wetting of all component porous volume is achieved. Wettability of the electrolyte into the electrode pores can be enhanced by lowering surface tension of electrolyte with an additive(s) or by increasing the composite surface energy of the electrode. Stable SEI formation also requires proper charge–discharge protocols that involve significant time due to slow charge rates between C/5 and C/20 [15]. Simply increasing charge rates for fast SEI formation results in incomplete, non-uniform, electrochemically unstable layers or deposits [121,171–173], thereby lowering cell efficiency, durability and safety. Similarly, insufficient electrolyte wetting leads to a low-quality SEI layer, inactive surface area, and/or premature cell performance degradation.

Electrolyte wetting and charge rate, particularly first-charge rate, are highly interlinked by a symbiotic electrochemical and mass transport relationship. In order to reduce formation time without losing cell performance, it is pertinent to fully review the current understanding of the SEI formation process, composition, morphology, structure, and their combined effects on both short-term (irreversible capacity loss) and long-term performance (capacity fade).

During SEI formation, lithium ions react at extremely electro-reducing potentials (close to 0 V vs. Li/Li^+) with electrolyte solvents and salts and anode electrons via electro-reduction reactions during charging. The reduced reactants precipitate and form the passive anode SEI layers, and reported reactions are enumerated in Table 2. SEI formation takes place mainly during first charging due to abundant electron availability to the electrolyte constituents because of negligible electrical resistance on the anode active material surface.

The reduction processes for EC and PC on a charging graphite anode are very similar, yielding similar SEI chemical compositions, but the layers behave differently during subsequent charge–discharge cycles (i.e. irreversible capacity loss and capacity fade) due to different bulk properties (i.e. thickness, porosity, tortuosity, etc.) of the reduction species [140,174,175].

An electrolyte system with $LiPF_6$ dissolved in an EC:DMC mixture is mostly stable above 1 V vs. Li/Li^+ [55,65,154], and no significant decomposition occurs. At potentials below 1 V vs. Li/Li^+, minor decomposition of the electrolyte species may occur, depending on the surface chemistry and morphology of graphite and the nature of electrolyte additives. Temperature and charge rate below this potential threshold also affect the decomposition reaction rates and products [113,114,125]. Disordered carbonaceous structures have a broader range of decomposition potentials than highly oriented ones because of differing reaction site energetics [64]. Graphite surface coatings or modifications can also alter the decomposition potential range. In some cases, minor amounts of highly resistive LiF precipitates can form in the SEI above 1 V vs. Li/Li^+ due to the stability of PF_5 in a compact polar solvent such as EC [92]. This LiF is sometimes detected during the early stages of electrolyte decomposition in nanometer-sized crystallites [55]. PF_5 is known as a strong Lewis acid that can also react with traces of water to produce HF, eliminate alkyl carbonate from lithium alkyl

Table 2
SEI formation and electrolyte decomposition reaction categories corresponding to reaction paths in Figs. 8–11.

	Reaction group	Reaction index
Ethylene carbonate (EC)	One-electron reduction	E1 [58,79,109,113,164], E2 [145,155], E3 [145,155], E4 [145,155], E5 [155], E6 [58,79,109,113], E7 [109], E8 [109]
	Two-electron reduction	E9 [155,165,166], E10 [58,62,66,79,109,150,155,165–167], E11 [55,145,155], E12 [55,60,62,79,91,125,155]
	Secondary reaction	E13 [145,168], E14 [145], E15 [145,167,168], E16 [145,167], E17 [145], E18 [145,167,168], E19 [165,166,168], E20 [125,166,169], E21 [62,166,170], E22 [17,145]
Propylene carbonate (PC)	One-electron reduction	P1 [37,58,126,164], P2 [109,126], P3 [37,126], P4 [37,42], P5 [58,109,126], P6 [109], P7 [109]
	Two-electron reduction	P8 [17,58], P9 [58,79,126], P10 [17,168]
	Secondary reaction	P11 [165,168], P12 [104,168], P13 [165,168], P14 [37,104,168], P15 [17,165,168], P16 [125,165,166], P17 [37], P18 [37], P19 [37]
Linear carbonate (LC)	One-electron reduction	L1 [166,167], L2 [164]
	Two-electron reduction	L3 [62,91], L4 [62,91]
	Secondary reaction	L5 [165,167,168], L6 [165,167,168], L7 [17], L8 [17,104,165,166,168,169], L9 [17,145]
Salt		S1 [17,91,92,145,165–170], S2 [17,55,165–167], S3 [17,60,145,165–169], S4 [165–168], S5 [17,91,92], S6 [91], S7 [91], S8 [17,42,60,104,165,168], S9 [17,42,104,165,168], S10 [17,42,104], S11 [165,166]

carbonate, and react with solvent carbonyl groups to produce insoluble ether-containing species [17,92,145]. At higher anode potentials, decomposition products like LiF are usually generated on graphite edge plane sites, which are preferable for nucleation due to a lower energy requirement than on basal plane sites. Fortunately LiF generation is kinetically slow and the amount of decomposition is small above 1 V vs. Li/Li^+.

It is well accepted that most of the SEI layer formation takes place within the potential range of 0.2–1.0 V vs. Li/Li^+. However, the formation mechanism(s) is highly debated. There have been two different concepts on the SEI formation process hypothesized, although their final structures are mostly alike. One concept follows a one-electron transfer to the electrolyte at high potential and a multi-electron transfer at low potential [55,145]. In other words, "bulk" lithium compounds (precipitates) are first partially reduced at high potential by a one-electron process due to insufficient electrons with low electron transfer resistance from electrode to electrolyte for complete reduction. At low potential, "compact" lithium compounds are generated from further reduction of pre-existing bulk lithium-containing precipitates on the anode surface, or directly by complete reduction of lithium compounds in electrolyte driven by high energy at low potential. The second concept supposes little or no precipitates preoccupying the anode graphite surface at high potential. Hence, electrons can transfer to electrolyte constituents without interference from resistive interfacial compounds. This high electron transfer rate induces compact lithium compound formation at higher potentials, and, as the potential is lowered and the decomposition layer thickens, electrolyte solvent molecules are gradually reduced. Subsequently, partially reduced bulk lithium compounds precipitate on top of the resistive compact layer to a greater extent as the potential reaches ~0.2 V vs. Li/Li^+.

Proponents of both hypotheses agree that major SEI formation begins around 0.8 V vs. Li/Li^+, but it can be higher for certain highly porous carbonaceous active materials [131]. In an ideal situation, the SEI formation will occur prior to lithium intercalation, which prevents co-intercalation of electrolyte constituents. For highly oriented graphite, lithium intercalation occurs at 0.2 V vs. Li/Li^+ or less, but it can start at slightly higher potentials in disordered or porous carbons [64,116,131]. Within the potential range of 0.6–0.8 V vs. Li/Li^+, electrons at the graphite surface transfer to the liquid electrolyte containing solvated lithium ions. These cations diffuse towards the graphite particles with an average of four strongly coordinated solvent molecules and an uncoordinated PF_6^- anion [118]. Uncoordinated solvent molecules are less likely to accept an electron because they are more stable than those associated with lithium ions. Most decomposition products from electro-reduction precipitate on the anode surfaces, while minor amounts diffuse back into the liquid phase and eventually re-precipitate elsewhere. Decomposition reactions prefer graphite edges because these sites usually include defects that are unstable and tend to be highly reactive. As the reaction rate on edge sites slows due to an increase in the coverage of precipitates, decomposition takes place on basal planes as well. These electrolyte decomposition reactions are irreversible and result in loss of lithium ions (cathode lithium inventory), solvent molecules, and salt anions (see Table 2 and Figs. 8–11) [145].

Below 0.6 V vs. Li/Li^+, a much greater extent of electrolyte decomposition takes place [55]. Dense inorganic lithium compound formation (i.e. LiO_2, Li_2CO_3 and LiF) is highly favorable at edge sites because of low electronic resistance to reducing solvent-coordinated lithium ions. Some less dense inorganic species such as lithium alkali carbonates and other organic species generally decompose on basal planes where reactions are less favorable. Since electronic resistance increases when a dense inorganic film is present on the graphite surfaces, subsequent decomposition onto the inorganic compounds will involve only partial reduction resulting in precipitation of loosely aggregated compounds such as lithium alkyl carbonates, or polymers. A portion of the lithium alkyl carbonate can be further reduced to form LiO_2 or Li_2CO_3 and release ethylene (from EC), propylene (from PC), or CO_2 gases [131]. The release of these gases may cause cracks in the existing SEI layer or even expose new anode graphite surface to electrolyte for further SEI decomposition reactions (further consuming lithium inventory).

A second or even third formation charging is usually needed to completely form a stable SEI layer for long LIB lifetimes. These subsequent charging half-cycles are often at progressively faster C rates.

10. Prospects for improving SEI properties and reducing formation time

Reducing LIB formation protocol time is necessary to lower production cost of cells (and ultimately packs) and manufacturing capital costs. The process currently lasts from about 4–5 days up to ~2 weeks depending on the cell chemistry, and it consumes a great deal of process energy (low-grade heat and electricity). In addition, it is also a substantial process bottleneck unless an inordinate amount of formation cyclers are used. SEI formation time can be reduced four ways: 1) by mixing additives into the electrolyte to form the SEI compounds more quickly and/or alter the overall composition of the SEI layer; 2) by modifying the anode graphite surface chemistry or substitution of the inactive binder and conductive additive materials with those having better wettability; 3) by charging and discharging the cells at higher rates within certain portions of the operating voltage window; and 4) by increasing the cell temperature during wetting and SEI formation.

Besides the popular vinyl carbonate (VC) additive, fluoroethylene carbonate, diphenyloctyl phosphate, acetyl caprolactam, 3-fluoro-1,3-propane sultone, prop-1-ene-1,3-sultone, and others have been proposed recently [112,123,153,154] These chemicals show different advantages over VC with respect to SEI composition and stability and cell lifetime, yet they have not been shown to save time during the formation cycling process. Developing or discovering an additive with an even higher reduction potential and high reactivity could result in reduced SEI formation time.

Anode active material surface coatings and chemical modifications can also improve SEI layer properties [144,176]. The volume change of carbonaceous materials during lithium intercalation is much lower when compared to other anode materials such as Al, Si, Sn, and Sb [43]. It has been found that an increase in disordered carbon anode surface oxygen resulted in low graphite exfoliation and stable SEI formation [135,143,177,178]. Using this property, a thin carbon coating on graphite can be implemented for improving capacity retention. Non-graphitic carbons do not undergo exfoliation to a great extent, but their first-cycle irreversible capacity loss is much higher due to greater surface area. When graphite is used without a carbon coating, reversible capacity is lower; however, once coated by a high-surface-area disordered carbon, reversible capacity increases because the majority of the SEI layer forms within the thin coating. This surface modification tends to prevent extensive graphite exfoliation [96,136,179].

It is plausible that SEI compounds differ not only depending on the reaction sites, such as edges vs. basal planes, but also depending on the initial surface elemental composition.

Initial precipitates on the non-oxidized graphite surfaces are likely different from those on oxidized surfaces, which could affect subsequent precipitation. Other surface modifications of various types of anode graphite have shown significant effects on SEI

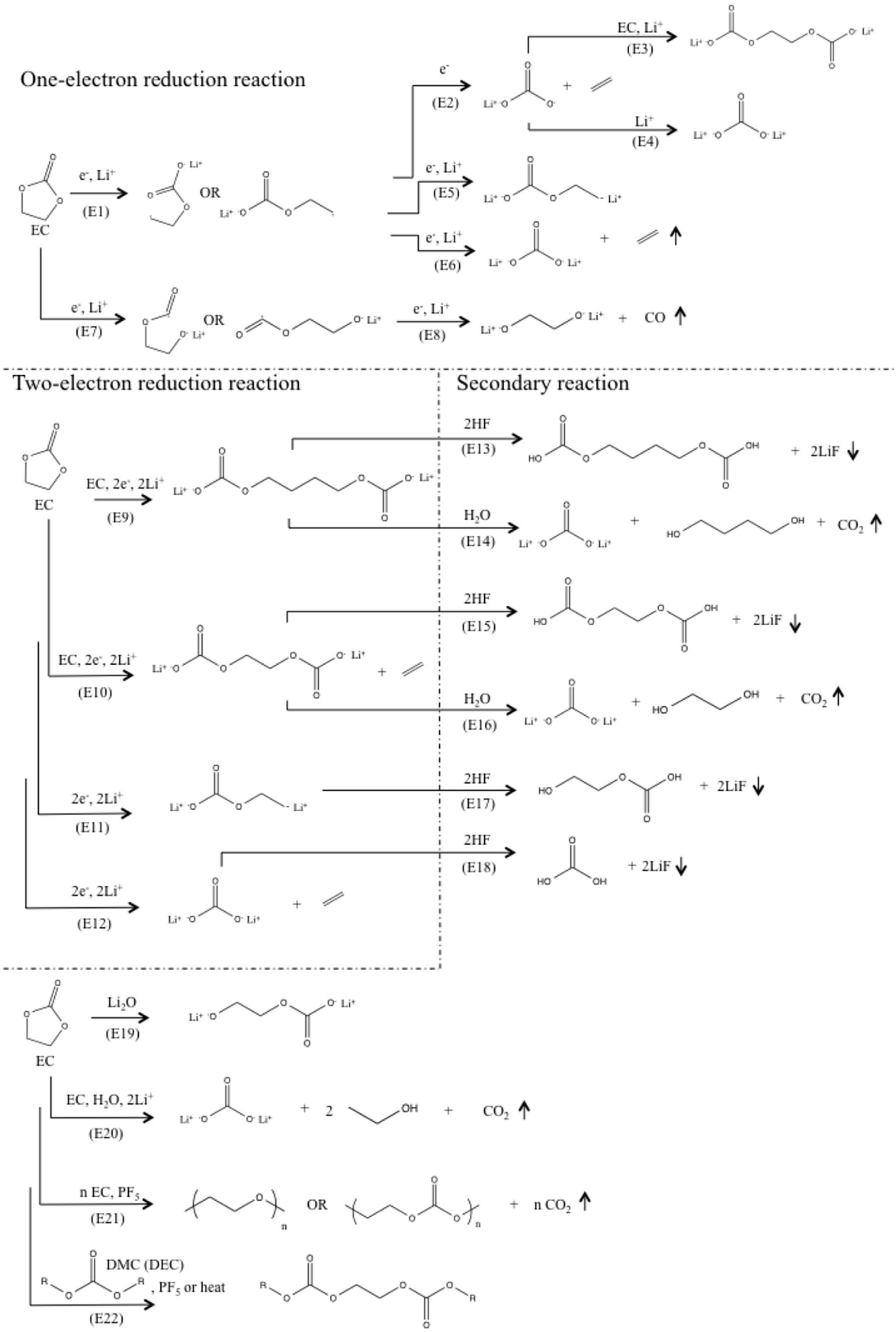

Fig. 8. Ethylene carbonate (EC) reduction process (reference groups in parentheses; details are shown in Table 2).

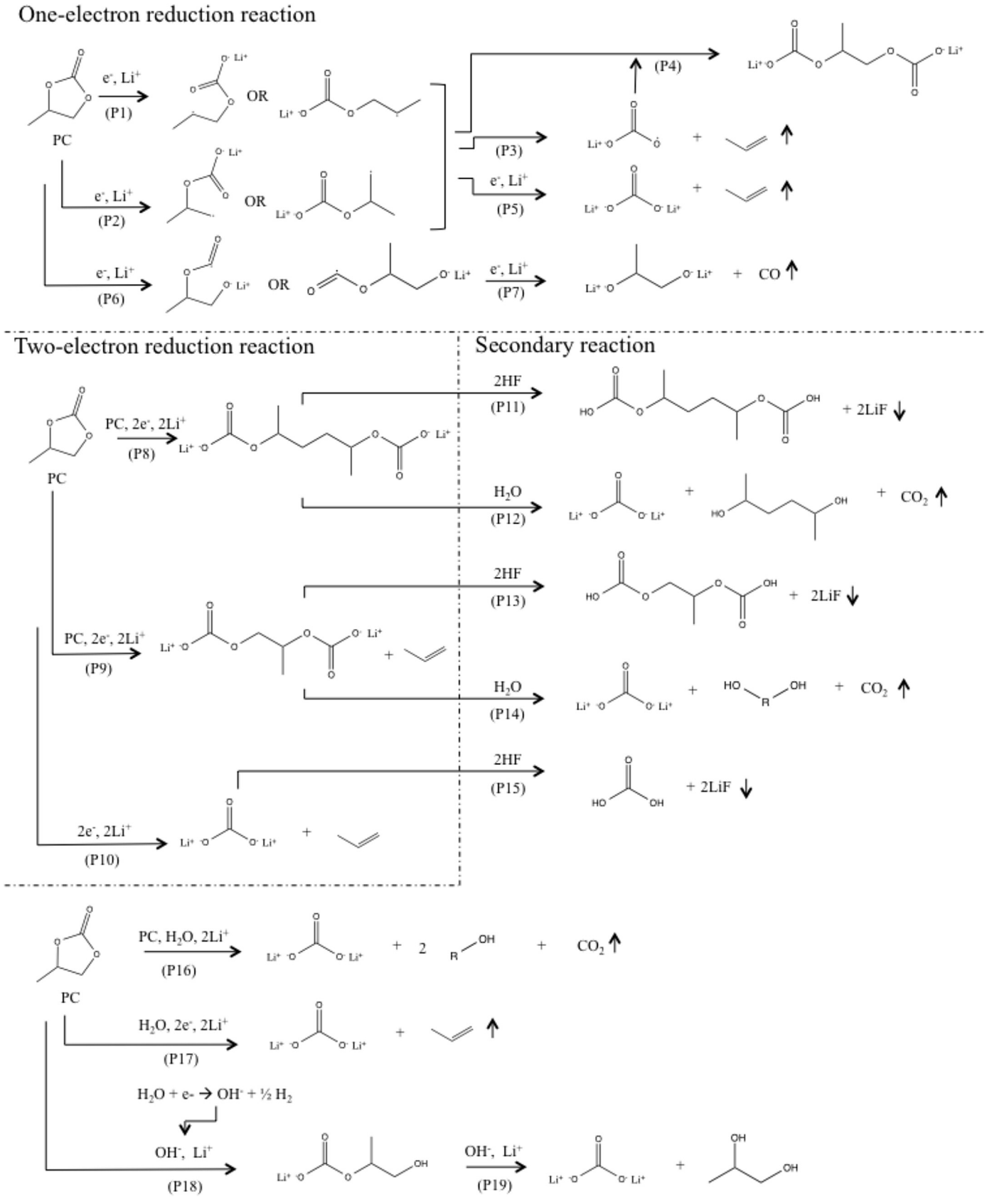

Fig. 9. Propylene carbonate (PC) reduction process (reference groups in parentheses; details are shown in Table 2).

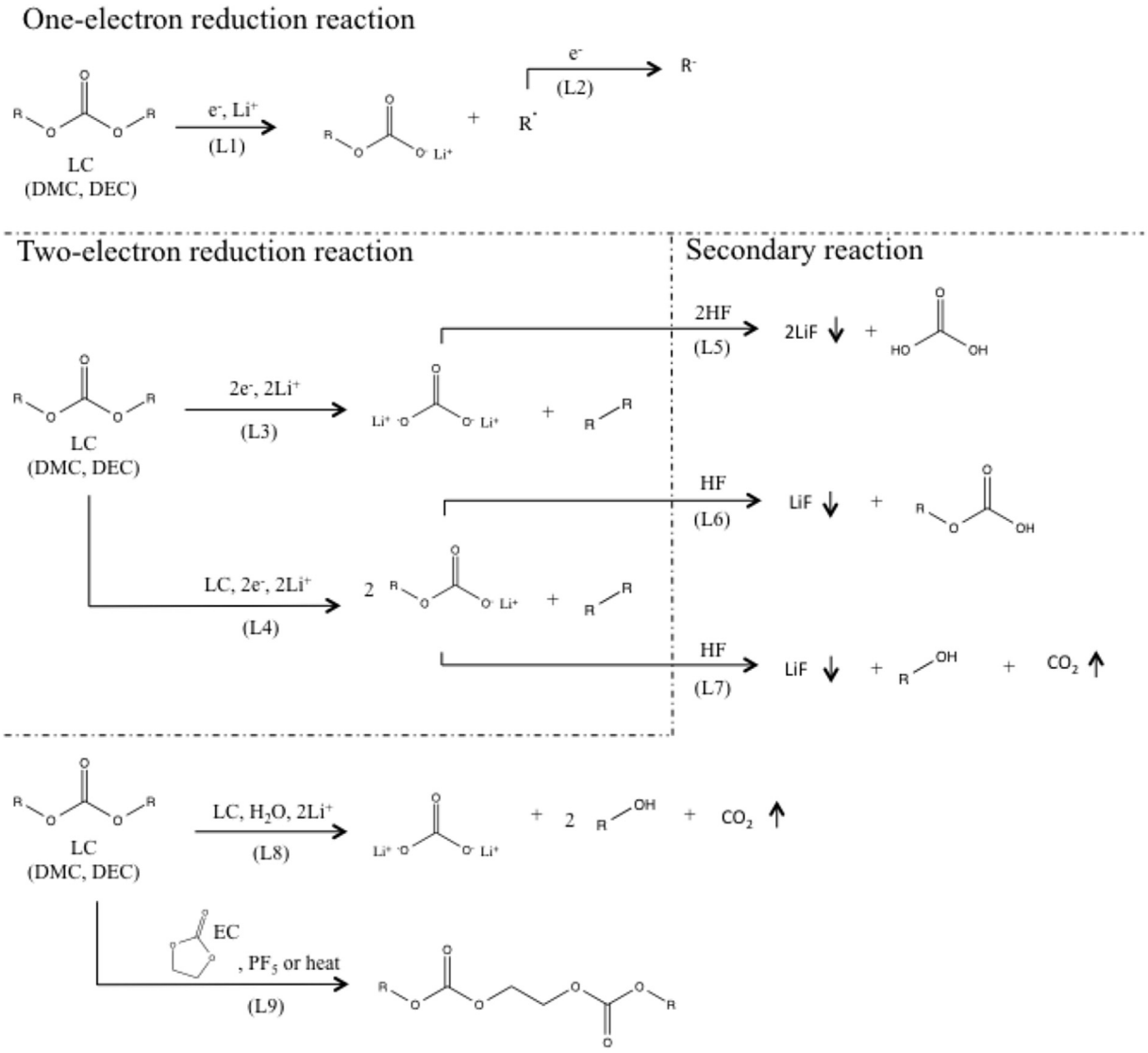

Fig. 10. Linear carbonate (LC) reduction process (reference groups in parentheses; details are shown in Table 2).

formation [93,94,136–138,179–181].

Generally, a high charging rate during the first cycle results in a porous and highly resistive SEI layer, while a low charging rate results in the opposite SEI characteristics. It has been found that for a 0.5C charging rate during SEI formation, capacity retention at room temperature operation was negatively affected [113]. Also, when the cell temperature was held above 40 °C, capacity retention was even more negatively affected for a 0.5C SEI formation charging rate [114]. Hence, a first charging rate between 0.05C and 0.2C is preferred for stable SEI formation. In some cases, though, high charging rate can be beneficial to SEI formation. For example, when TIMREX® SFG44 graphite was heat-treated in an inert gas at 3000 °C, a high charge current of 320 mA/g (~1C), showed better reversible capacity in 1 M $LiPF_6$ EC/DMC than a much lower charge current of 10 mA/g (~0.03C) [122]. In this case, high current decomposed the electrolyte faster than solvents could intercalate into graphene sheets and cause exfoliation. Low charging rates may be beneficial for SEI formation, but they slow cell production rates and increase production cost and plant capital expense. Building a stable SEI with a charging rate greater than 0.5C may require a great deal of further effort on developing proper additives, optimizing cell temperature, and modifying the anode surface chemistry.

At higher temperatures, SEI formation may also be accelerated. SEI layers formed at temperatures around 40 °C tend to have more compact lithium precipitates, such as Li_2CO_3 and Li_2O, rather than softer, organic precipitates like $ROCO_2Li$. However, high temperature may induce LiF precipitation from fluorine containing salts.

11. Recent progress in SEI layer studies and prospects for future understanding

11.1. Computational studies

11.1.1. Overview of molecular dynamics (MD) and density functional theory (DFT) studies

Molecular dynamics (MD) and density functional theory (DFT) simulation methods have been used to understand the intricate relationship between the SEI layer and electrolyte. The MD approach uses atomic force calculations through solving Newton's equations of motion and investigates dynamic movements and equilibrium of atoms and molecules primarily with potentials from semi-empirical relationships. While MD has provided detailed information on classical many-body problems, ab-initio molecular dynamics (AIMD) has extended MD capability by combining the

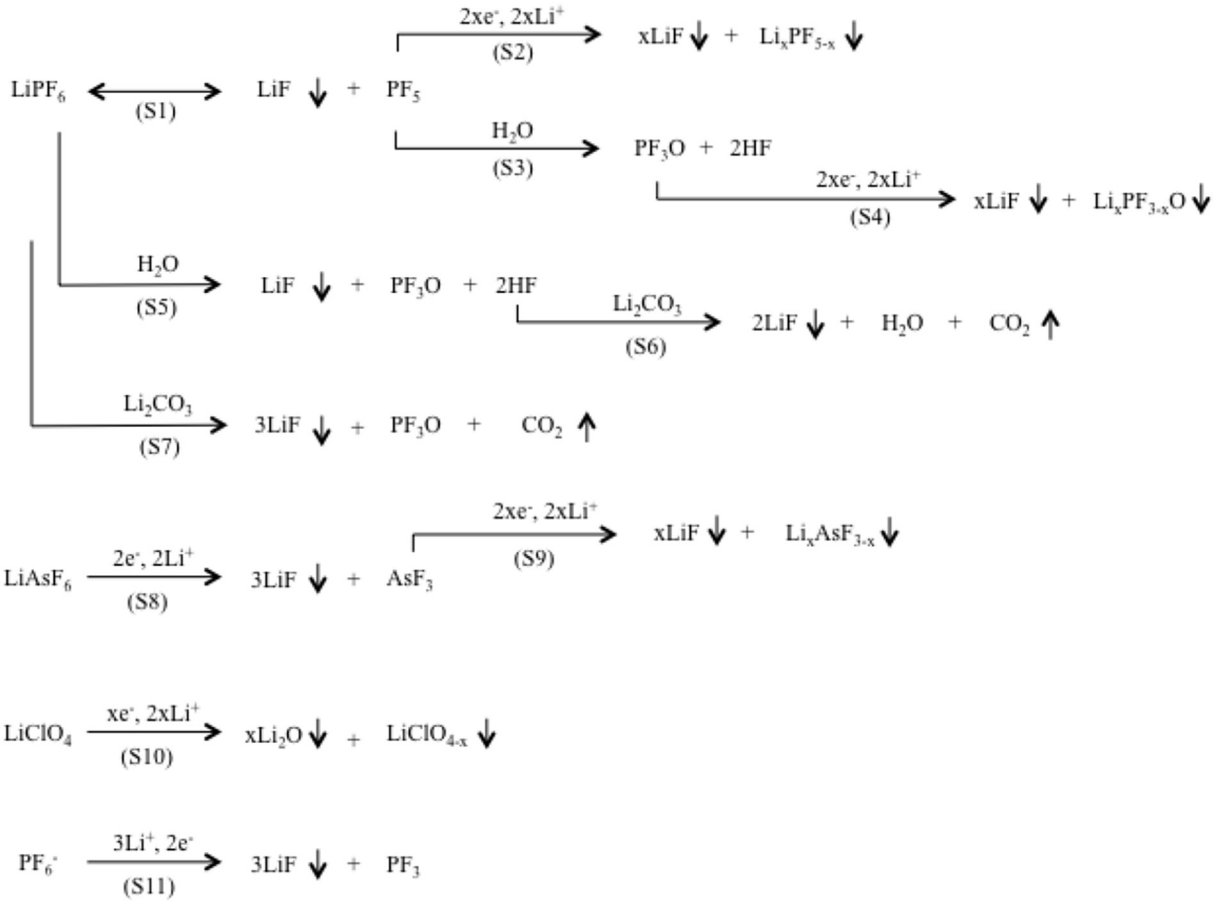

Fig. 11. Electrolyte salt reduction process (reference groups in parentheses; details are shown in Table 2).

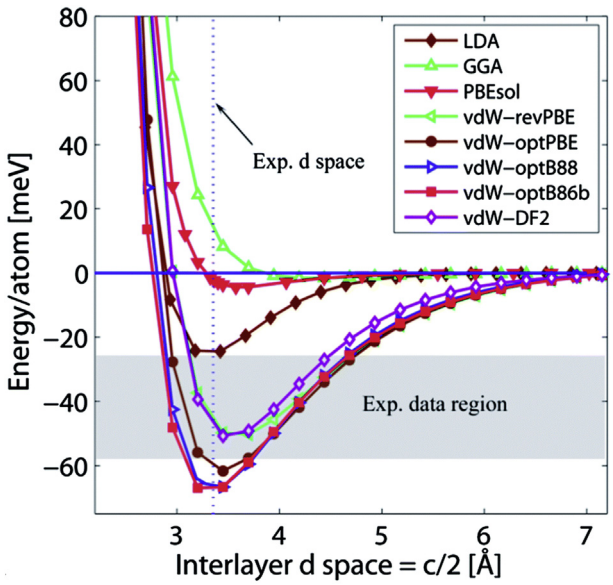

Fig. 12. Interlayer binding energy of graphite as a function of interlayer separation calculated by LDA, GGA and five different vdW functionals [192]. Reproduced from Ref. 192 with permission from The Royal Society of Chemistry. (A colour version of this figure can be viewed online.)

Schrödinger wave equation with Newton's equations. Certain interfacial reduction and oxidation reactions have been described in the literature using AIMD [182–188]. APPLE&P (Atomistic Polarizable Potential for Liquids, Electrolytes, & Polymers) is another many-body polarizable force field for MD simulations that can capture electrostatic interactions in polarizable environments. Binding energies between lithium ions and solvent molecules may vary with different theory levels of APPLE&P force fields. For example, M05-2X and B3LYP are common levels, which are thought to have overestimated lithium-ion/$MECO_3^-$ binding energy in lithium alkyl carbonate electrolytes. The M06-L, MP2, and G4MP2 levels, on the other hand, have shown similar, and more reasonable, binding energies [189–191].

Density functional theory (DFT) is more rigorous than MD, and the former is another computational approach in quantum mechanics that solves Schrödinger equation. It estimates the electronic structures in atomic and molecular systems, but it is limited to smaller simulation sizes than MD because of the associated computational intensity. One of the issues in using DFT is weak van-der-Waals-like forces of graphene layers, which can affect calculations for lithium-ion/solvent-molecule co-intercalation into graphite. Computed graphene interlayer binding energy significantly varies depending on DFT functionals [192]. Local-density approximation (LDA), a well-known and simple functional, underestimates the binding energy of graphite interlayer as shown in Fig. 12. The binding energies from experiments were 31–52 meV/atom [193–195]. Another issue in using quantum simulations is that the simulations are typically not suitable for estimating competing reactions.

DFT and MD mainly deal with Angstrom and nanometer length scales, respectively. Because of the small length scales and heavy

calculation load, it is extremely difficult to fully combine electrode, SEI layer, electrolyte, and all of their interactions together into a single model. Hence, the computational literature on SEI formation and physical chemistry is comprised of reactions and molecular coordination of lithium ions with one or two types of molecules. In this section, some of the SEI-related calculations are discussed.

11.1.2. Correlation of SEI with graphite

Jorn et al. performed ab initio molecular dynamics simulations with graphite in $LiPF_6$/EC electrolytes, while considering graphite basal and edge planes [196]. In this study, the SEI layer was composed of Li_2EDC (lithium ethylene dicarbonate) only or Li_2EDC with different amounts of LiF. They found that edge planes could accommodate more Li ions than basal planes due to the broad range of EC orientations, which might cause different SEI formation processes and structures at the two types of reaction sites. Thicker SEI layers or higher HF contents in the electrolyte resulted in a higher lithium ion concentration in the vicinity of the SEI surface, promoting higher probability of lithium ion transport from solvent to SEI. DFT calculations also showed that irreversible capacity loss (ICL) on graphite surfaces, generally on edges, having dangling bonds is higher than that on graphite surfaces having H-terminated edges [197]. This finding perhaps implies greater SEI formation thickness due to unstable graphite edges. Surface properties of graphite may also affect adhesion of the SEI to the graphite surfaces. DFT-MD simulations were carried out with probable SEI film components from EC-based electrolyte (Li_2EDC) to see their adhesion to graphite having H-terminations [198]. It was found that the adhesion to the H-terminated graphite was unstable in EC. Dissolution energies of Li_2EDC in EC were +12.2 kcal/mol.

There have been other computational approaches to understanding SEI formation and lithium-ion/solvent co-intercalation into graphene layers. DFT and MD simulations showed that half-distances between C–C (graphene) interlayers were 0.59 nm for $Li^+(EC)C_{72}$, 0.69 nm for $Li^+(EC)_4C_{72}$, 0.70 nm for $Li^+(PC)C_{72}$, and 0.85 nm for $Li^+(PC)_4C_{72}$ when no ring openings of EC or PC were assumed [199]. Half-distances between C–C interlayers were 0.325–0.335 nm with no lithium ions or solvent molecules and 0.356–0.376 nm for LiC_6 [199–202]. If there were ring openings of EC or PC, the difference between the associated EC and PC C–C distances would be little because the PC methyl group would have free rotation after the ring opening. For the case where the PC and EC molecules would not undergo ring opening during co-intercalation, $Li^+(PC)_n$ and $Li^+(EC)_n$ could cause graphite disintegration by widening the C–C layers (which experience only weak van der Waals forces), and since $Li^+(PC)_n$ is more massive than $Li^+(EC)_n$, the probability of this disintegration process could be higher for $Li^+(PC)_n$ than $Li^+(EC)_n$.

11.1.3. Reduction reactions

Most reduction processes take place between 0.9 V and 0.2 V vs Li/Li^+ on highly ordered graphite, but salt products may decompose at higher voltages according to one DFT study. LiF formation, deposition, and radical recombination were found to occur near 2 V vs Li/Li^+ before the main solvent reduction reactions below 0.9 V vs. Li/Li^+ for FEC or below 0.6 V vs. Li/Li^+ for EC [203]. In the case of EC and PC based electrolytes, reduction energies of $Li^+(EC)_4$ were 8 kcal/mol lower than $Li^+(PC)_4$ [199], which implies that $Li^+(EC)_n$ is more prone to reduction than $Li^+(PC)_n$. Statistical and surface analyses also showed that smaller molecular-weight compounds and salt decomposed on the anode surfaces in the presence of electrolyte, followed by long-chain oligomer compounds [204–206].

For the case of 1 M $LiPF_6$ with different binary solvents such as EC:EMC, EC:DMC, or EC:DEC (1:2 volume ratio), in-situ experiments showed the released gases were in the following order of amount: $C_2H_4 > CO > CH_4 > C_2H_6 > CO_2$ [207]. Contrary to these experimental findings of greater CO than CO_2, a particular DFT study showed different results [208]. Calculations using the hybrid-level functionals B3LYP with basis set 6-311++G(d,p) showed that EC strongly coordinated with the PF_6^- anion and was prone to oxidation to the EC radical cation on cathode via 1-electron transfer. The EC radical cation was subsequently reduced on the anode and produced CO_2, aldehyde, and oligomers of alkyl carbonates. CO_2 was generated to a greater extent than CO due to the high activation energy for CO.

Regarding the common VC additive, DFT based MD simulations from Ushirogata et al. showed that VC reacted with an EC anion radical causing a one-electron reduction of EC [182], which implies that VC assists the EC reduction process. Although exactly how VC decomposes is not yet clear, experimental and computational agreement has been found that VC increases solvent reduction reaction rates.

11.1.4. SEI layer composition and ion diffusion

A molecular dynamics study from Kim et al. showed that Li_2CO_3 and Li_2O were the main SEI components on anodes when EC and DMC were used as the electrolyte solvents [51]. SEI layers were found to form at about 1 V vs. Li/Li^+, and they were composed primarily of inorganic components close to the anode surface and primarily of organic ones close to the liquid electrolyte. In these simulations, however, lithium metal was considered as the anode instead of graphite. It should also be noted that the presence of electrolyte salts were not considered, and reaction gas products from the inner portion of the SEI were not allowed to diffuse outward into the liquid phase (these gases would be removed under real-world formation conditions). Hence, actual SEI layers are composed of somewhat different compounds than these particular calculated ones.

Lithium ion transport in Li_2EDC, a common component of SEI layers, was studied by EIS experiments and MD simulations with APPLE&P force field and G4MP2 and MP2 levels [189]. The conductivity of Li_2EDC at room temperature was found to be 10^{-9} S/cm from EIS analysis and 2×10^{-10}–10^{-8} S/cm from MD simulation. The calculated activation energy ranged from 64 to 84 kJ/mol at 393 K, indicating that lithium ion transport exhibited a hopping mechanism at high temperature.

11.2. SEI on anode metalloid or metal oxide

Metalloid or metal oxides, especially SiO_x and SnO_x, are regarded as prime candidate materials for high-energy batteries due to high theoretical capacity and earth abundance [209–211], despite Si and Sn having higher operating potentials than graphite (around 0.4 V and 0.6 V vs. Li/Li^+, respectively). One of main problems, however, is that these two materials suffer from extreme volume changes during lithium intercalation and deintercalation, leading to: 1) extensive, unstable, and thick SEI formation; 2) poor long-term mechanical properties; and 3) severe capacity fade.

In order to build stable SEI layers on these materials, research has concentrated on a combined materials approach such as Si alloys [52,209,210,212], Sn alloys [213–216], Si–C or Sn–C composites [213,217–230], Sn or Si composited with carbon nanomaterials [231–239], Mo–C or Ni–C [240–244], or mixing with graphene [245–247]. For these solutions, volumetric capacities drop to half of those of pure Si or Sn, but the reductions in capacity still result in anodes with much higher specific capacities than graphite. Volume changes on these composited and blended materials also become smaller, making the formed SEI layers more chemically stable and longer lasting. Coating Al_2O_3 on these materials also mitigates volume changes [248,249].

Lithium metal is also being reconsidered as a possible anode candidate because it has the highest specific capacity, but it suffers from significant safety concerns related to lithium dendrite growth into and through the separator (electrical shorting). One reason this degradation and potential failure mechanism occurs is because the SEI layer is not uniform and tough enough to prevent dendrite growth. Some of the proposed ways to prevent lithium dendrite growth are hollow carbon nanospheres covering surface of lithium anode, adopting an alternative salt, and electrolyte additives [250–252].

11.3. Additives

Some additives having fluorine can also improve SEI formation on metal anode materials. For example, FEC has moved to the forefront as an attractive additive since it improves SEI layer properties and cell cycle life of metal anode systems [253,254]. It is especially effective when the when the metal particles are nanoscale [255]. Studies on understanding FEC's effect on metal anode formation mechanisms are currently ongoing [183,256,257].

In general, most additive research focuses on forming stable and robust SEI layers. Zhu et al., on the other hand, used polyfluoroalkyl compounds as an additive to build a micelle-like SEI layer on an anode electrode. The heads of the additive decompose on the electrode surfaces and solvophobic tails point outwards towards the electrolyte [258]. They found 4-(perfluorooctyl)-1,3-dioxolan-2-one improved capacity retention and lowered impedance in high voltage lithium ion batteries. These pre-formed SEI layers were found to protect the cathode from electrolyte decomposition as well as the anode. They also tested lithium difluorooxalatoborate, triphenylamine, and 1,4-benzodiozane-6,7-diol as a combined additive and obtained improved capacity retention and lowered impedance for a $Li_{1.2}Ni_{0.15}Mn_{0.55}Co_{0.1}O_2$ (TODA HE5050)/graphite cell [259].

PC as an electrolyte solvent has excellent properties with the exception of exfoliating the graphite during unstable SEI formation. Wagner et al. improved anode SEI formation by using methyl vinyl sulfone (MVS) and ethyl vinyl sulfone (EVS) additives in PC [260]. These additives decomposed on graphite and built protective SEI layers before PC could intercalate and react because MVS and EVS have 1.3 eV and 1.2 eV lower LUMO energies, respectively, than PC. Unlike these “active” additives that decompose on the anode, there are other additives that prevent decomposition during cycling. For example, Chrétien et al. mixed both LiF and glyme additives ($CH_3O[CH_2CH_2O]_nCH_3$) in the electrolyte to inhibit side reactions [261]. Glymes and lithium salt compounds are more electrochemically stable than ethers and have high oxidation potentials close to 4.7 V, allowing high-voltage operation with NMC.

11.4. Prospects for future understanding

LIBs for high energy or high power demands like vehicle application require high capacity, high capacity retention, high voltage operation, low cost, low weight and volume, etc. All of these requirements are deeply related to SEI layers. Regarding capacity and capacity retention during the first few charge cycles, batteries lose approximately 10–15% of their capacity due to initial anode SEI formation. Afterword, irreversible capacity loss continues due to gradual SEI deposition during long-term cycling, although it is far less than the loss during initial SEI formation. The capacity loss percentage and initial SEI properties vary depending on formation conditions such as anode material surface area, surface properties of the material, anode-to-cathode capacity ratio, temperature, charge rate, charge depth, surface properties of the anode materials, salt/solvent properties, additives, and impurities. Detailed information about the effects of these properties and conditions can be found in previous sections of this paper.

High-voltage operation of LIBs does not significantly affect anode SEI formation directly, but it does have indirect effects. Cathode materials designed for operation at high cell potential (i.e. overcharged NMC or LMR-NMC) release cathode constituents (mostly Mn, some Ni, and a minor amount of Co) into the electrolyte that diffuse through the separator to the anode side, and in turn, induce more SEI formation by increasing the electron conductivity of SEI layer. High-voltage operation of cells also causes electrolyte instability (oxidation) on the cathode surfaces, and a SEI-like layer forms at the cathode that is chemically less stable than its anode counterpart. Hence, under these cell operating conditions, cell impedance increases due to both changes in the anode SEI layer and excessive growth of the cathode SEI layer.

12. Summary

This paper comprehensively reviews the science of SEI layer formation on carbon/graphite anode surfaces in the LIBs, including structure, morphology, chemical composition, electrochemistry, formation mechanism, and formation cycling. In order to develop shorter, more robust LIB formation protocols, which are needed to reduce cell manufacturing cost and battery plant capital investment, a thorough understanding of the relationship between state-of-the-art SEI layer compositions and capacity fade are still needed. Furthermore, new formation protocols which develop ideal SEI layers (those that consume minimal lithium inventory during formation and reduce capacity fade during long-term cell operation) in shorter time periods will require an understanding of SEI layer evolution over the LIB life, a subject which is currently not well understood.

It is understood and accepted, however, that the SEI is formed by the decomposition products of the electrolyte solvent molecules and lithium salt, and it critically affects the short-term and long-term performance of the cell. The importance of the SEI layer was given in terms of first-cycle efficiency, capacity retention, and cell cost, as well as the state of understanding of the SEI formation mechanism and methods of analysis and characterization. Various factors that affect SEI formation were also discussed such as anode materials, surface properties, formation current density, electrolyte additives, and cell temperature.

The anode SEI layer covers the graphite surfaces and shields lithium ions from the electrolyte solution, which prevents further electrolyte decomposition. This shielding property enables reversible capacity during extended charge–discharge cycling. However, the SEI formation process consumes lithium ions and electrolyte when generated, resulting in first-cycle irreversible capacity and lithium inventory losses. This irreversible capacity loss may continue if the SEI is not well formed by hindering electrolyte diffusion or allowing unwanted electron transfer from the graphite to the liquid phase.

SEI compositions and morphologies are complicated and differ depending on graphite surface properties, electrolyte, and formation conditions. Several modeling and experimental efforts are underway to address the correct pathways of these electroreduction reactions and elucidate the debate within the LIB research community. SEI analysis is a challenging task due to its thickness being only ~3–100 nm and its delicate nature. A variety of traditional experimental techniques have been used for the electrochemical, morphological, and chemical analysis of the SEI layer.

The morphology and chemical makeup of an SEI is unique to the specific graphite surface and electrolyte solution pair, but it can generally be thought of as consisting of three layers: an outer porous, less-compact layer formed from the organic compounds

near the liquid electrolyte zone; an inner more-compact inorganic structure adjacent to the graphite surface; and an intermixed layer with intermediate properties between the inner and outer layers.

Acknowledgments

This research at Oak Ridge National Laboratory, managed by UT Battelle, LLC, for the U.S. Department of Energy (DOE) under contract DE-AC05-00OR22725, was sponsored by the Office of Energy Efficiency and Renewable Energy (EERE) Vehicle Technologies Office (VTO) (Acting Program Director: David Howell) Applied Battery Research subprogram (Program Manager: Peter Faguy).

References

[1] J.B. Goodenough, K.-S. Park, The Li-ion rechargeable battery: a perspective, J. Am. Chem. Soc. 135 (4) (2013) 1167–1176, http://dx.doi.org/10.1021/ja3091438.
[2] D. Mohanty, J. Li, R. Born, L.C. Maxey, et al., Non-destructive evaluation of slot-die-coated lithium secondary battery electrodes by in-line laser caliper and IR thermography methods, Anal. Methods 6 (3) (2014) 674, http://dx.doi.org/10.1039/c3ay41140k.
[3] D. Mohanty, A. Huq, E.A. Payzant, A.S. Sefat, et al., Neutron diffraction and magnetic susceptibility studies on a high-voltage Li1.2Mn0.55Ni0.15-Co0.10O2 lithium ion battery cathode: insight into the crystal structure, Chem. Mater. 25 (20) (2013) 4064–4070, http://dx.doi.org/10.1021/cm402278q.
[4] J. Li, B.L. Armstrong, C. Daniel, J. Kiggans, et al., Optimization of multicomponent aqueous suspensions of lithium iron phosphate (LiFePO4) nanoparticles and carbon black for lithium-ion battery cathodes, J. Colloid Interface Sci. 405 (2013) 118–124, http://dx.doi.org/10.1016/j.jcis.2013.05.030.
[5] J. Li, B.L. Armstrong, J. Kiggans, C. Daniel, et al., Lithium ion cell performance enhancement using aqueous LiFePO4 cathode dispersions and polyethyleneimine dispersant, J. Electrochem. Soc. 160 (2) (2012) A201–A206, http://dx.doi.org/10.1149/2.037302jes.
[6] J. Li, C. Daniel, D.L. Wood, Materials processing for lithium-ion batteries, J. Power Sources 196 (2011) 2452–2460, http://dx.doi.org/10.1016/j.jpowsour.2010.11.001.
[7] C. Daniel, Materials and processing for lithium-ion batteries, J. Miner. Metals Mater. Soc. 60 (2008) 43–48, http://dx.doi.org/10.1007/s11837-008-0116-x.
[8] J.R. Croy, A. Abouimrane, Z. Zhang, Next-generation lithium-ion batteries: the promise of near term advancements, MRS Bull. 39 (05) (2014) 407–415, http://dx.doi.org/10.1557/mrs.2014.84.
[9] S.S. Zhang, Status, opportunities, and challenges of electrochemical energy storage, Front. Energy Res. 1 (2013) 1–6, http://dx.doi.org/10.3389/fenrg.2013.00008.
[10] J.-M. Tarascon, M. Armand, Building better batteries, Nature 451 (2008) 652–657, http://dx.doi.org/10.1038/451652a.
[11] M.S. Whittingham, Lithium batteries and cathode materials, Chem. Rev. 104 (2004) 4271–4301, http://dx.doi.org/10.1021/cr020731c.
[12] J. Li, C. Rulison, J. Kiggans, C. Daniel, et al., Superior performance of LiFePO4 aqueous dispersions via corona treatment and surface energy optimization, J. Electrochem. Soc. 159 (8) (2012) A1152–A1157, http://dx.doi.org/10.1149/2.018208jes.
[13] D.L. Wood, J. Li, D. Mohanty, C. Daniel, et al., Advanced materials processing and novel characterization methods for low-cost, high energy-density lithium-ion batteries, in: Advanced Automotive Battery Conference, 2013.
[14] D. Mohanty, A.S. Sefat, J. Li, R.A. Meisner, et al., Correlating cation ordering and voltage fade in a lithium-manganese-rich lithium-ion battery cathode oxide: a joint magnetic susceptibility and TEM study, Phys. Chem. Chem. Phys. PCCP 15 (44) (2013) 19496–19509, http://dx.doi.org/10.1039/c3cp53658k.
[15] D.L. Wood, J. Li, C. Daniel, Prospects for reducing the processing cost of lithium ion batteries, J. Power Sources 275 (2015) 234–242, http://dx.doi.org/10.1016/j.jpowsour.2014.11.019.
[16] N.C. Gallego, C.I. Contescu, H.M. Meyer, J.Y. Howe, et al., Advanced surface and microstructural characterization of natural graphite anodes for lithium ion batteries, Carbon 72 (2014) 393–401, http://dx.doi.org/10.1016/j.carbon.2014.02.031.
[17] K. Xu, Nonaqueous liquid electrolytes for lithium-based rechargeable batteries, Chem. Rev. 104 (2004) 4303–4417, http://dx.doi.org/10.1021/cr030203g.
[18] A. Patil, V. Patil, D.W. Shin, J.-W. Choi, et al., Issue and challenges facing rechargeable thin film lithium batteries, Mater. Res. Bull. 43 (2008) 1913–1942, http://dx.doi.org/10.1016/j.materresbull.2007.08.031.
[19] R. Yazami, Y.F. Reynier, Mechanism of self-discharge in graphite–lithium anode, Electrochim. Acta 47 (2002) 1217–1223, http://dx.doi.org/10.1016/S0013-4686(01)00827-1.
[20] R. Yazami, Surface chemistry and lithium storage capability of the graphite-lithium electrode, Electrochim. Acta 45 (1999) 87–97, http://dx.doi.org/10.1016/S0013-4686(99)00195-4.
[21] J.B. Goodenough, Y. Kim, Challenges for rechargeable Li batteries, Chem. Mater. 22 (2010) 587–603, http://dx.doi.org/10.1021/cm901452z.
[22] M. Wohlfahrt-Mehrens, C. Vogler, J. Garche, Aging mechanisms of lithium cathode materials, J. Power Sources 127 (1–2) (2004) 58–64, http://dx.doi.org/10.1016/j.jpowsour.2003.09.034.
[23] J. Vetter, P. Novák, M.R. Wagner, C. Veit, et al., Ageing mechanisms in lithium-ion batteries, J. Power Sources 147 (1–2) (2005) 269–281, http://dx.doi.org/10.1016/j.jpowsour.2005.01.006.
[24] D. Mohanty, S. Kalnaus, R.A. Meisner, K.J. Rhodes, et al., Structural transformation of a lithium-rich Li1.2Co0.1Mn0.55Ni0.15O2 cathode during high voltage cycling resolved by in situ X-ray diffraction, J. Power Sources 229 (2013) 239–248, http://dx.doi.org/10.1016/j.jpowsour.2012.11.144.
[25] D. Mohanty, A.S. Sefat, S. Kalnaus, J. Li, et al., Investigating phase transformation in the Li1.2Co0.1Mn0.55Ni0.15O2 lithium-ion battery cathode during high-voltage hold (4.5 V) via magnetic, X-ray diffraction and electron microscopy studies, J. Mater. Chem. A 1 (20) (2013) 6249, http://dx.doi.org/10.1039/c3ta10304h.
[26] Z. Lu, D.D. MacNeilb, J.R. Dahn, Layered cathode materials Li[NixLi(1/3–2x/3)Mn(2/3–x/3)]O2 for lithium-ion batteries, Electrochem. Solid State Lett. 4 (11) (2001) A191–A194, http://dx.doi.org/10.1149/1.1407994.
[27] M.M. Thackeray, C.S. Johnson, J.T. Vaughey, N. Li, et al., Advances in manganese-oxide 'composite' electrodes for lithium-ion batteries, J. Mater. Chem. 15 (2005) 2257–2267, http://dx.doi.org/10.1039/B417616M.
[28] N. Yabuuchi, K. Yoshii, S.-T. Myung, I. Nakai, et al., Detailed studies of a high-capacity electrode material for rechargeable batteries, Li2MnO3–LiCo1/3Ni1/3Mn1/3O2, J. Am. Chem. Soc. 133 (2011) 4404–4419, http://dx.doi.org/10.1021/ja108588y.
[29] S. Krueger, R. Kloepsch, J. Li, S. Nowak, et al., How do reactions at the anode/electrolyte interface determine the cathode performance in lithium-ion batteries? J. Electrochem. Soc. 160 (2013) A542–A548, http://dx.doi.org/10.1149/2.022304jes.
[30] K. Amine, C.H. Chen, J. Liu, M. Hammond, et al., Factors responsible for impedance rise in high power lithium ion batteries, J. Power Sources 97–98 (2001) 684–687, http://dx.doi.org/10.1016/S0378-7753(01)00701-7.
[31] G. Sarre, P. Blanchard, M. Broussely, Aging of lithium-ion batteries, J. Power Sources 127 (1–2) (2004) 65–71, http://dx.doi.org/10.1016/j.jpowsour.2003.09.008.
[32] M. Broussely, P. Biensan, F. Bonhomme, P. Blanchard, et al., Main aging mechanisms in Li ion batteries, J. Power Sources 146 (1–2) (2005) 90–96, http://dx.doi.org/10.1016/j.jpowsour.2005.03.172.
[33] R. Kostecki, F. McLarnon, Degradation of LiNi[sub 0.8]Co[sub 0.2]O[sub 2] cathode surfaces in high-power lithium-ion batteries, Electrochem. Solid State Lett. 5 (7) (2002) A164–A166, http://dx.doi.org/10.1149/1.1482199.
[34] M. Shikano, H. Kobayashi, S. Koike, H. Sakaebe, et al., Investigation of positive electrodes after cycle testing of high-power Li-ion battery cells II, J. Power Sources 174 (2) (2007) 795–799, http://dx.doi.org/10.1016/j.jpowsour.2007.06.138.
[35] M.K. Rahman, Y. Saito, Investigation of positive electrodes after cycle testing of high-power Li-ion battery cells, J. Power Sources 174 (2) (2007) 889–894, http://dx.doi.org/10.1016/j.jpowsour.2007.06.222.
[36] V. Etacheri, R. Marom, R. Elazari, G. Salitra, et al., Challenges in the development of advanced Li-ion batteries: a review, Energy Environ. Sci. 4 (2011) 3243–3262, http://dx.doi.org/10.1039/c1ee01598b.
[37] D. Aurbach, H. Gojxjeb, The electrochemical behavior of selected polar aprotic systems, Electrochem. Acta 34 (1989) 141–156, http://dx.doi.org/10.1016/0013-4686(89)87079-3.
[38] A. Wursig, H. Buqa, M. Holzapfel, F. Krumeich, et al., Film formation at positive electrodes in lithium-ion batteries, Electrochem. Solid State Lett. 8 (2005) A34–A37, http://dx.doi.org/10.1149/1.1836114.
[39] J.Y. Song, H.H. Lee, Y.Y. Wang, C.C. Wan, Two- and three-electrode impedance spectroscopy of lithium-ion batteries, J. Power Sources 111 (2002) 255–267, http://dx.doi.org/10.1016/S0378-7753(02)00310-5.
[40] N. Williard, B. Sood, M. Osterman, M. Pecht, Disassembly methodology for conducting failure analysis on lithium–ion batteries, J. Mater. Sci. Mater. Electron. 22 (10) (2011) 1616–1630, http://dx.doi.org/10.1007/s10854-011-0452-4.
[41] F. Orsini, A. Du Pasquier, B. Beaudoin, J.M. Tarascon, et al., In situ scanning electron microscopy (SEM) observation of interfaces within plastic lithium batteries, J. Power Sources 76 (1998) 19–29, http://dx.doi.org/10.1016/S0378-7753(98)00128-1.
[42] O.Y. Chusid, Y. Ein Ely, D. Aurbach, M. Babai, et al., Electrochemical and spectroscopic studies of carbon electrodes in lithium battery electrolyte systems, J. Power Sources 43–44 (1993) 47–64, http://dx.doi.org/10.1016/0378-7753(93)80101-T.
[43] B. Scrosati, Garche Jr., Lithium batteries: status, prospects and future, J. Power Sources 195 (2010) 2419–2430, http://dx.doi.org/10.1016/j.jpowsour.2009.11.048.
[44] E. Markevich, G. Salitra, K. Fridman, R. Sharabi, et al., Fluoroethylene carbonate as an important component in electrolyte solutions for high-voltage lithium batteries: role of surface chemistry on the cathode, Langmuir ACS J. Surf. Colloids 30 (25) (2014) 7414–7424, http://dx.doi.org/10.1021/la501368y.
[45] M. Xu, N. Tsiouvaras, A. Garsuch, H.A. Gasteiger, et al., Generation of cathode

passivation films via oxidation of lithium bis(oxalato) borate on high voltage spinel (LiNi0.5Mn1.5O4), J. Phys. Chem. C 118 (14) (2014) 7363–7368, http://dx.doi.org/10.1021/jp501970j.
[46] H. Bouayad, Z. Wang, N. Dupré, R. Dedryvère, et al., Improvement of electrode/electrolyte interfaces in high-voltage spinel lithium-ion batteries by using glutaric anhydride as electrolyte additive, J. Phys. Chem. C 118 (9) (2014) 4634–4648, http://dx.doi.org/10.1021/jp5001573.
[47] X. Li, Y. Chen, C.C. Nguyen, M. Nie, et al., Stability of inactive components of cathode laminates for lithium ion batteries at high potential, J. Electrochem. Soc. 161 (4) (2014) A576–A582, http://dx.doi.org/10.1149/2.060404jes.
[48] P. Verma, P. Maire, P. Novak, A review of the features and analyses of the solid electrolyte interphase in Li-ion batteries, Electrochim. Acta 55 (2010) 6332–6341, http://dx.doi.org/10.1016/j.electacta.2010.05.072.
[49] D. Aurbach, M.D. Levi, E. Levi, A. Schechter, Failure and stabilization mechanisms of graphite electrodes, J. Phys. Chem. B 101 (1997) 2195–2206, http://dx.doi.org/10.1021/jp962815t.
[50] K. Tasaki, S.J. Harris, Computational study on the solubility of lithium salts formed on lithium ion battery negative electrode in organic solvents, J. Phys. Chem. C 114 (2010) 8076–8083, http://dx.doi.org/10.1021/jp100013h.
[51] S.-P. Kim, A.C.T.V. Duin, V.B. Shenoy, Effect of electrolytes on the structure and evolution of the solid electrolyte interphase (SEI) in Li-ion batteries: a molecular dynamics study, J. Power Sources 196 (20) (2011) 8590–8597, http://dx.doi.org/10.1016/j.jpowsour.2011.05.061.
[52] J. Zheng, H. Zheng, R. Wang, L. Ben, et al., 3D visualization of inhomogeneous multi-layered structure and Young's modulus of the solid electrolyte interphase (SEI) on silicon anodes for lithium ion batteries, Phys. Chem. Chem. Phys. PCCP 16 (26) (2014) 13229–13238, http://dx.doi.org/10.1039/c4cp01968g.
[53] M. Nie, B.L. Lucht, Role of lithium salt on solid electrolyte interface (SEI) formation and structure in lithium ion batteries, J. Electrochem. Soc. 161 (6) (2014) A1001–A1006, http://dx.doi.org/10.1149/2.054406jes.
[54] N. Takenaka, Y. Suzuki, H. Sakai, M. Nagaoka, On electrolyte-dependent formation of solid electrolyte interphase film in lithium-ion batteries: strong sensitivity to small structural difference of electrolyte molecules, J. Phys. Chem. C 118 (20) (2014) 10874–10882, http://dx.doi.org/10.1021/jp5018696.
[55] P. Lu, C. Li, E.W. Schneider, S.J. Harris, Chemistry, impedance, and morphology evolution in solid electrolyte interphase films during formation in lithium ion batteries, J. Phys. Chem. C 118 (2014) 896–903, http://dx.doi.org/10.1021/jp4111019.
[56] S.J. Harris, P. Lu, Effects of Inhomogeneities—nanoscale to mesoscale—on the durability of Li-ion batteries, J. Phys. Chem. C 117 (2013) 6481–6492, http://dx.doi.org/10.1021/jp311431z.
[57] M. Nie, D. Chalasani, D.P. Abraham, Y. Chen, et al., Lithium ion battery graphite solid electrolyte interphase revealed by microscopy and spectroscopy, J. Phys. Chem. C 117 (3) (2013) 1257–1267, http://dx.doi.org/10.1021/jp3118055.
[58] S. Tsubouchi, Y. Domi, T. Doi, M. Ochida, et al., Spectroscopic characterization of surface films formed on edge plane graphite in ethylene carbonate-based electrolytes containing film-forming additives, J. Electrochem. Soc. 159 (2012) A1786–A1790, http://dx.doi.org/10.1149/2.028211jes.
[59] E. Peled, D. Golodnitsky, C. Menachem, D. BarTow, An advanced tool for the selection of electrolyte components for rechargeable lithium batteries, J. Electrochem. Soc. 145 (1998) 3482–3486, http://dx.doi.org/10.1149/1.1838831.
[60] V. Eshkenazi, E. Peled, L. Burstein, D. Golodnitsky, XPS analysis of the SEI formed on carbonaceous materials, Solid State Ion. 170 (1–2) (2004) 83–91, http://dx.doi.org/10.1016/s0167-2738(03)00107-3.
[61] E. Peled, D. Golodnitsky, A. Ulus, V. Yufit, Effect of carbon substrate on SEI composition and morphology, Electrochim. Acta 50 (2–3) (2004) 391–395, http://dx.doi.org/10.1016/j.electacta.2004.01.130.
[62] S. Leroy, H. Martinez, R. Dedryve're, D. Lemordant, et al., Influence of the lithium salt nature over the surface film formation on a graphite electrode in Li-ion batteries: an XPS study, Appl. Surf. Sci. 253 (2007) 4895–4905, http://dx.doi.org/10.1016/j.apsusc.2006.10.071.
[63] E. Peled, D. Golodnitsky, G. Ardel, Advanced model for solid electrolyte interphase electrodes in liquid and polymer electrolyte, J. Electrochem. Soc. 144 (1997) L208–L210, http://dx.doi.org/10.1149/1.1837858.
[64] K. Naoi, N. Ogihara, Y. Igarashi, A. Kamakura, et al., Disordered carbon anode for lithium-ion battery – I. An interfacial reversible redox action and anomalous topology changes, J. Electrochem. Soc. 152 (2005) A1047–A1053, http://dx.doi.org/10.1149/1.1896531.
[65] A. Tokranov, B.W. Sheldon, P. Lu, X. Xiao, et al., The origin of stress in the solid electrolyte interphase on carbon electrodes for Li ion batteries, J. Electrochem. Soc. 161 (2014) A58–A65, http://dx.doi.org/10.1149/2.009401jes.
[66] H.-L. Zhang, F. Li, C. Liu, J. Tan, et al., New insight into the solid electrolyte interphase with use of a focused ion beam, J. Phys. Chem. B 109 (2005) 22205–22211, http://dx.doi.org/10.1021/jp053311a.
[67] D. Aurbach, Review of selected electrode–solution interactions which determine the performance of Li and Li ion batteries, J. Power Sources 89 (2000) 206–218, http://dx.doi.org/10.1016/S0378-7753(00)00431-6.
[68] S. Mori, H. Asahina, H. Suzuki, A. Yonei, et al., Chemical properties of various organic electrolytes for lithium rechargeable batteries: 1. Characterization of passivating layer formed on graphite in alkyl carbonate solutions, J. Power Sources 68 (1997) 59–64, http://dx.doi.org/10.1016/S0378-7753(97)02619-0.
[69] D. Aurbach, M. Moshkovich, A Study of lithium deposition-dissolution processes in a few selected electrolyte solutions by electrochemical quartz crystal microbalance, J. Electrochem. Soc. 145 (1998) 2629–2639, http://dx.doi.org/10.1149/1.1838692.
[70] E. Peled, D. Bar Tow, A. Merson, A. Gladkich, et al., Composition, depth profiles and lateral distribution of materials in the SEI built on HOPG-TOF SIMS and XPS studies, J. Power Sources 97–98 (2001) 52–57, http://dx.doi.org/10.1016/S0378-7753(01)00505-5.
[71] A. Augustsson, M. Herstedt, J.H. Guo, K. Edstrom, et al., Solid electrolyte interphase on graphite Li-ion battery anodes studied by soft X-ray spectroscopy, Phys. Chem. Chem. Phys. 6 (2004) 4185–4189, http://dx.doi.org/10.1039/B313434B.
[72] D. Aurbach, Electrode–solution interactions in Li-ion batteries: a short summary and new insights, J. Power Sources 119–121 (2003) 497–503, http://dx.doi.org/10.1016/S0378-7753(03)00273-8.
[73] E. Peled, D. Golodnitsky, C. Menachem, D. BarTow, An advanced tool for the selection of electrolyte components for rechargeable lithium batteries, J. Electrochem. Soc. 145 (1998) 3482–3486, http://dx.doi.org/10.1149/1.1838831.
[74] D. Aurbach, Y. Einely, A. Zaban, The surface chemistry of lithium electrodes in alkyl carbonate solutions, J. Electrochem. Soc. 141 (1994) L1–L3, http://dx.doi.org/10.1149/1.2054718.
[75] K.-I. Morigaki, A. Ohta, Analysis of the surface of lithium in organic electrolyte by atomic force microscopy, Fourier transform infrared spectroscopy and scanning auger electron microscopy, J. Power Sources 76 (1998) 159–166, http://dx.doi.org/10.1016/S0378-7753(98)00151-7.
[76] D. Bar-Tow, E. Peled, L. Burstein, A study of highly oriented pyrolytic graphite as a model for the graphite anode in Li-ion batteries, J. Electrochem. Soc. 146 (1999) 824–832, http://dx.doi.org/10.1149/1.1391688.
[77] K. Kanamura, H. Tamura, Z. Takehara, In-situ electrogeneration of [2,2′-ethylenebis(nitrilomethylidyne)diphenolato]nickelate(I)—nickel(I) salen—as a catalyst for reductive intramolecular cyclizations of 6-iodo- and 6-bromo-1-phenyl-1-hexyne, J. Electroanal. Chem. 333 (1992) 127–134, http://dx.doi.org/10.1016/0022-0728(92)80345-5.
[78] M. Odziemkowski, D.E. Irish, An electrochemical study of the reactivity at the lithium electrolyte/bare lithium metal interface: II. Unpurified Solvents, J. Electrochem. Soc. 140 (1993) 1546–1555, http://dx.doi.org/10.1149/1.2221600.
[79] D. Aurbach, B. Markovsky, I. Weissman, E. Levi, et al., On the correlation between surface chemistry and performance of graphite negative electrodes for Li ion batteries, Electrochim. Acta 45 (1999) 67–86, http://dx.doi.org/10.1016/S0013-4686(99)00194-2.
[80] A. Kominato, E. Yasukawa, N. Sato, T. Ijuuin, et al., Analysis of surface films on lithium in various organic electrolytes, J. Power Sources 68 (1997) 471–475, http://dx.doi.org/10.1016/S0378-7753(97)02592-5.
[81] A.D. Pasquier, F. Disma, T. Bowmer, A.S. Gozdz, et al., Differential scanning calorimetry study of the reactivity of carbon anodes in plastic Li-ion batteries, J. Electrochem. Soc. 145 (1998) 472–477, http://dx.doi.org/10.1149/1.1838287.
[82] H.H. Lee, C.C. Wan, Y.Y. Wang, Thermal stability of the solid electrolyte interface on carbon electrodes of lithium batteries, J. Electrochem. Soc. 151 (2004) A542–A547, http://dx.doi.org/10.1149/1.1647568.
[83] D. Aurbach, Y. Gofer, M. Benzion, P. Aped, The behaviour of lithium electrodes in propylene and ethylene carbonate: Te major factors that influence Li cycling efficiency, J. Electroanal. Chem. 339 (1992) 451–471, http://dx.doi.org/10.1016/0022-0728(92)80467-I.
[84] G.R. Zhuang, Y.F. Chen, P.N. Ross, The reaction of lithium with dimethyl carbonate and diethyl carbonate in ultrahigh vacuum studied by X-ray photoemission spectroscopy, Langmuir ACS J. Surf. Colloids 15 (1999) 1470–1479, http://dx.doi.org/10.1021/la980454y.
[85] D. Alliata, R. Kotz, P. Novák, H. Siegenthaler, Electrochemical SPM investigation of the solid electrolyte interphase film formed on HOPG electrodes, Electrochem. Commun. 2 (2000) 436–440, http://dx.doi.org/10.1016/S1388-2481(00)00056-4.
[86] M.N. Richard, J.R. Dahn, Accelerating rate calorimetry study on the thermal stability of lithium intercalated graphite in electrolyte. I. Experimental, J. Electrochem. Soc. 146 (1999) 2068–2077, http://dx.doi.org/10.1149/1.1391893.
[87] D.D. MacNeil, D. Larcher, J.R. Dahn, Comparison of the reactivity of various carbon electrode materials with electrolyte at elevated temperature, J. Electrochem. Soc. 146 (1999) 3596–3602, http://dx.doi.org/10.1149/1.1392520.
[88] F. Joho, P. Novák, M.E. Spahr, Safety aspects of graphite negative electrode materials for lithium-ion batteries, J. Electrochem. Soc. 149 (2002) A1020–A1024, http://dx.doi.org/10.1149/1.1488915.
[89] D. Aurbach, Y. Cohen, The application of atomic force microscopy for the study of Li deposition processes, J. Electrochem. Soc. 143 (1996) 3525–3532, http://dx.doi.org/10.1149/1.1837248.
[90] D. Aurbach, M.L. Daroux, P.W. Faguy, E. Yeager, Identification of surface films formed on lithium in propylene carbonate solutions, J. Electrochem. Soc. 134 (1987) 1611–1620, http://dx.doi.org/10.1149/1.2100722.
[91] S. Leroy, F. Blanchard, R. Dedryvere, H. Martinez, et al., Surface film formation on a graphite electrode in Li-ion batteries: AFM and XPS study, Surf. Interface

Anal. 37 (10) (2005) 773–781, http://dx.doi.org/10.1002/Sia.2072.
[92] K. Tasaki, K. Kanda, S. Nakamura, M. Ue, Decomposition of LiPF6 and stability of PF5 in Li-ion battery electrolytes, J. Electrochem. Soc. 150 (2003) A1628–A1636, http://dx.doi.org/10.1149/1.1622406.
[93] E. Peled, C. Menachem, D. Bar-Tow, A. Melman, Improved graphite anode for lithium-ion batteries, chemically bonded solid electrolyte interface and nanochannel formation, J. Electrochem. Soc. 143 (1995) L4–L7, http://dx.doi.org/10.1149/1.1836372.
[94] A.J. Loebl, C.J. Oldham, C.K. Devine, B. Gong, et al., Solid electrolyte interphase on lithium-ion carbon nanofiber electrodes by atomic and molecular layer deposition, J. Electrochem. Soc. 160 (2013) A1971–A1978, http://dx.doi.org/10.1149/2.020311jes.
[95] S.-K. Jeong, M. Inaba, T. Abe, Z. Ogumi, Surface film formation on graphite negative electrode in lithium-ion batteries: AFM study in an ethylene carbonate-based solution, J. Electrochem. Soc. 148 (2001) A989–A993, http://dx.doi.org/10.1149/1.1387981.
[96] P. Bernardo, J.M. Le Meins, L. Vidal, J. Dentzer, et al., Influence of graphite edge crystallographic orientation on the first lithium intercalation in Li-ion battery, Carbon 91 (2015) 458–467, http://dx.doi.org/10.1016/j.carbon.2015.05.001.
[97] S. Bhattacharya, A.R. Riahi, A.T. Alpas, Thermal cycling induced capacity enhancement of graphite anodes in lithium-ion cells, Carbon 67 (2014) 592–606, http://dx.doi.org/10.1016/j.carbon.2013.10.032.
[98] J. Yan, J. Zhang, Y.-C. Su, X.-G. Zhang, et al., A novel perspective on the formation of the solid electrolyte interphase on the graphite electrode for lithium-ion batteries, Electrochim. Acta 55 (2010) 1785–1794, http://dx.doi.org/10.1016/j.electacta.2009.10.068.
[99] M. Park, X. Zhang, M. Chung, G.B. Less, et al., A review of conduction phenomena in Li-ion batteries, J. Power Sources 195 (2010) 7904–7929, http://dx.doi.org/10.1016/j.jpowsour.2010.06.060.
[100] E. Endo, M. Ata, K. Tanaka, K. Sekai, Electron spin resonance study of the electrochemical reduction of electrolyte solutions for lithium secondary batteries, J. Electrochem. Soc. 145 (1998) 3757–3764, http://dx.doi.org/10.1149/1.1838870.
[101] A.N. Dey, B.P. Sullivan, The electrochemical decomposition of propylene carbonate on graphite, J. Electrochem. Soc. 117 (1970) 222, http://dx.doi.org/10.1149/1.2407470.
[102] J.O. Besenhard, M. Winter, J. Yang, W. Biberacher, Filming mechanism of lithium-carbon anodes in organic and inorganic electrolytes, J. Power Sources 54 (1995) 228–231, http://dx.doi.org/10.1016/0378-7753(94)02073-C.
[103] G.-C. Chung, H.-J. Kim, S.-I. Yu, S.-H. Jun, et al., Origin of graphite exfoliation an investigation of the important role of solvent cointercalation, J. Electrochem. Soc. 147 (2000) 4391–4398, http://dx.doi.org/10.1149/1.1394076.
[104] D. Aurbach, A. Zaban, Impedance spectroscopy of lithium electrodes-part 1-general behavior in propylene carbonate solutions and the correlation to surface chemistry and cycling efficiency, J. Electroanal. Chem. 348 (1993) 155–179, http://dx.doi.org/10.1016/0022-0728(93)80129-6.
[105] D. Aurbach, K. Gamolsky, B. Markovsky, Y. Gofer, et al., On the use of vinylene carbonate (VC) as an additive to electrolyte solutions for Li-ion batteries, Electrochim. Acta 47 (2002) 1423–1439.
[106] D. Aurbach, Y. Gofer, J. Langzam, The correlation between surface chemistry, surface morphology, and cycling efficiency of lithium electrodes in a few polar aprotic systems, J. Electrochem. Soc. 136 (1989) 3198–3205, http://dx.doi.org/10.1149/1.2096425.
[107] S.D. Reeves, R.S. Morris, Improved MCMB anodes by surface modification with self-assembling nonionic surfactants, Electrochem. Solid State Lett. 7 (2004) B29–B30, http://dx.doi.org/10.1149/1.1764412.
[108] C. Wang, A.J. Appleby, F.E. Little, Irreversible capacities of graphite anode for lithium-ion batteries, J. Electroanal. Chem. 519 (2002) 9–17, http://dx.doi.org/10.1016/S0022-0728(01)00708-2.
[109] K. Xu, Whether EC and PC differ in interphasial chemistry on graphitic anode and how, J. Electrochem. Soc. 156 (2009) A751–A755, http://dx.doi.org/10.1149/1.3166182.
[110] C. Marino, A. Darwiche, N. Dupre, H.A. Wilhelm, et al., Study of the electrode/electrolyte interface on cycling of a conversion type electrode material in Li batteries, J. Phys. Chem. C 117 (2013) 19302–19313, http://dx.doi.org/10.1021/jp402973h.
[111] H.-H. Lee, Y.-Y. Wang, C.-C. Wan, M.-H. Yang, et al., A fast formation process for lithium batteries, J. Power Sources 134 (2004) 118–123, http://dx.doi.org/10.1016/j.jpowsour.2004.03.020.
[112] I.-J. Park, T.-H. Nam, J.-G. Kim, Diphenyloctyl phosphate as a solid electrolyte interphase forming additive for Li-ion batteries, J. Power Sources 244 (2013) 122–128, http://dx.doi.org/10.1016/j.jpowsour.2013.03.031.
[113] C. Huang, K. Huang, H. Wang, S. Liu, et al., The effect of solid electrolyte interface formation conditions on the aging performance of Li-ion cells, J. Solid State Electrochem. 15 (2011) 1987–1995, http://dx.doi.org/10.1007/s10008-010-1219-1.
[114] Y.-B. He, B. Li, Q.-H. Yang, H. Du, et al., Effects of current densities on the formation of LiCoO2/graphite lithium ion battery, J. Solid State Electrochem. 15 (2011) 1977–1985, http://dx.doi.org/10.1007/s10008-010-1220-8.
[115] J. Lei, L. Li, R. Kostecki, R. Muller, et al., Characterization of SEI layers on LiMn2O4 cathodes with in situ spectroscopic ellipsometry, J. Electrochem. Soc. 152 (2005) A774–A777, http://dx.doi.org/10.1149/1.1867652.
[116] M.-S. Zheng, Q.-F. Dong, H.-Q. Cai, M.-G. Jin, et al., Formation and influence factors of solid electrolyte interphase film on the negative electrode surface in lithium-ion batteries, J. Electrochem. Soc. 152 (2005) A2207–A2210, http://dx.doi.org/10.1149/1.2060669.
[117] H. Tavassol, J.W. Buthker, G.A. Ferguson, L.A. Curtiss, et al., Solvent oligomerization during SEI formation on model systems for Li-ion battery anodes, J. Electrochem. Soc. 159 (2012) A730–A738, http://dx.doi.org/10.1149/2.067206jes.
[118] M. Nie, D.P. Abraham, D.M. Seo, Y. Chen, et al., Role of solution structure in solid electrolyte interphase formation on graphite with LiPF6 in propylene carbonate, J. Phys. Chem. C 117 (2013) 25381–25389, http://dx.doi.org/10.1021/jp409765w.
[119] L. Wang, X. Deng, P.-X. Dai, Y.-G. Guo, et al., Initial solid electrolyte interphase formation process of graphite anode in LiPF6 electrolyte: an in situ ECSTM investigation, Phys. Chem. Chem. Phys. 14 (2012) 7330–7336, http://dx.doi.org/10.1039/c2cp40595d.
[120] S.H. Ng, C. Vix-Guterl, P. Bernardo, N. Tran, et al., Correlations between surface properties of graphite and the first cycle specific charge loss in lithium-ion batteries, Carbon 47 (2009) 705–712, http://dx.doi.org/10.1016/j.carbon.2008.11.008.
[121] S. Bhattacharya, A.T. Alpas, Micromechanisms of solid electrolyte interphase formation on electrochemically cycled graphite electrodes in lithium-ion cells, Carbon 50 (2012) 5359–5371, http://dx.doi.org/10.1016/j.carbon.2012.07.009.
[122] W. Markle, C.-Y. Lu, P. Novák, Morphology of the solid electrolyte interphase on graphite in dependency on the formation current, J. Electrochem. Soc. 158 (2011) A1478–A1482, http://dx.doi.org/10.1149/2.077112jes.
[123] B. Li, Y. Wang, H. Rong, Y. Wang, et al., A novel electrolyte with the ability to form a solid electrolyte interface on the anode and cathode of a LiMn2O4/graphite battery, J. Mater. Chem. A 1 (2013) 12954–12961, http://dx.doi.org/10.1039/c3ta13067c.
[124] M. Herstedt, A.M. Andersson, H. Rensmo, H. Siegbahn, et al., Characterisation of the SEI formed on natural graphite in PC-based electrolytes, Electrochim. Acta 49 (2004) 4939–4947, http://dx.doi.org/10.1016/j.electacta.2004.06.006.
[125] S.-B. Lee, S.-I. Pyun, The effect of electrolyte temperature on the passivity of solid electrolyte interphase formed on a graphite electrode, Carbon 40 (2002) 2333–2339, http://dx.doi.org/10.1016/S0008-6223(02)00144-6.
[126] L. Zhu, F. Hommet, G. Salace, B. Claude-Montigny, et al., STM observation of the electro-adsorption of lithium ions onto graphite and of the ensuing solid electrolyte interphase formation, Surf. Sci. 512 (2002) 84–96, http://dx.doi.org/10.1016/S0039-6028(02)01576-5.
[127] Z. Zeng, W.-I. Liang, H.-G. Liao, H.L. Xin, et al., Visualization of electrode–electrolyte interfaces in LiPF6/EC/DEC electrolyte for lithium ion batteries via in situ TEM, Nano Lett. 14 (2014) 1745–1750, http://dx.doi.org/10.1021/nl403922u.
[128] M. Gu, L.R. Parent, B.L. Mehdi, R.R. Unocic, et al., Demonstration of an electrochemical liquid cell for operando transmission electron microscopy observation of the lithiation/delithiation behavior of Si nanowire battery anodes, Nano Lett. 13 (2013) 6106–6112, http://dx.doi.org/10.1021/nl403402q.
[129] B.L. Mehdi, M. Gu, L.R. Parent, W. Xu, et al., In-situ electrochemical transmission electron microscopy for battery research, Microsc. Microanal. 20 (2014) 484–492, http://dx.doi.org/10.1017/S1431927614000488.
[130] J.E. Owejan, J.P. Owejan, S.C. DeCaluwe, J.A. Dura, Solid electrolyte interphase in Li-ion batteries: evolving structures measured in situ by neutron reflectometry, Chem. Mater. 24 (2012) 2133–2140, http://dx.doi.org/10.1021/cm3006887.
[131] C.A. Bridges, X.-G. Sun, J. Zhao, M.P. Paranthaman, et al., In situ observation of solid electrolyte interphase formation in ordered mesoporous hard carbon by small-angle neutron scattering, J. Phys. Chem. C 116 (2012) 7701–7711, http://dx.doi.org/10.1021/jp3012393.
[132] F. Joho, B. Rykart, A. Blome, P. Novák, Relation between surface properties, pore structure and first-cycle charge loss of graphite as negative electrode in lithium-ion batteries, J. Power Sources 97 (2001) 78–82, http://dx.doi.org/10.1016/S0378-7753(01)00595-X.
[133] M. Li, Y. Wu, F. Zhao, Y. Wei, et al., Cycle and rate performance of chemically modified super-aligned carbon nanotube electrodes for lithium ion batteries, Carbon 69 (2014) 444–451, http://dx.doi.org/10.1016/j.carbon.2013.12.047.
[134] P. Novák, J. Ufheil, H. Buqa, F. Krumeich, et al., The importance of the active surface area of graphite materials in the first lithium intercalation, J. Power Sources 174 (2007) 1082–1085, http://dx.doi.org/10.1016/j.jpowsour.2007.06.036.
[135] M.E. Spahr, H. Wilhelm, T. Palladino, N. Dupont-Pavlovsky, et al., The role of graphite surface group chemistry on graphite exfoliation during electrochemical lithium insertion, J. Power Sources 119–121 (2003) 543–549, http://dx.doi.org/10.1016/s0378-7753(03)00284-2.
[136] M. Yoshio, H. Wang, K. Fukuda, Y. Hara, et al., Effect of carbon coating on electrochemical performance of treated natural graphite as lithium-ion battery anode material, J. Electrochem. Soc. 147 (2000) 1245–1250, http://dx.doi.org/10.1149/1.1393344.
[137] Y. Wu, C. Jiang, C. Wan, E. Tsuchida, Effects of catalytic oxidation on the electrochemical performance of common natural graphite as an anode material for lithium ion batteries, Electrochem. Commun. 2 (2000) 272–275, http://dx.doi.org/10.1016/S1388-2481(00)00022-9.
[138] Y.P. Wu, C. Jiang, C. Wan, R. Holze, Anode materials for lithium ion batteries

by oxidative treatment of common natural graphite, Solid State Ion. 156 (2003) 283–290, http://dx.doi.org/10.1016/S0167-2738(02)00680-X.
[139] J. Rafiee, X. Mi, H. Gullapalli, A.V. Thomas, et al., Wetting transparency of graphene, Nat. Mater. 11 (2012) 217–222, http://dx.doi.org/10.1038/nmat3228.
[140] E. Peled, The electrochemical behavior of alkali and alkaline earth metals in nonaqueous battery systems-the solid electrolyte interphase model, J. Electrochem. Soc. 126 (1979) 2047–2051, http://dx.doi.org/10.1149/1.2128859.
[141] J. Christensen, J. Newman, A mathematical model for the lithium-ion negative electrode solid electrolyte interphase, J. Electrochem. Soc. 151 (2004) A1977–A1988, http://dx.doi.org/10.1149/1.1804812.
[142] A.M. Colclasure, K.A. Smith, R.J. Kee, Modeling detailed chemistry and transport for solid-electrolyte-interface (SEI) films in Li–ion batteries, Electrochim. Acta 58 (2011) 33–43, http://dx.doi.org/10.1016/j.electacta.2011.08.067.
[143] Y. Ein-Eli, V.R. Koch, Chemical oxidation: a route to enhanced capacity in Li-ion graphite anodes, J. Electrochem. Soc. 144 (1997) 2968–2973, http://dx.doi.org/10.1149/1.1837945.
[144] J. Collins, G. Gourdin, M. Foster, D. Qu, Carbon surface functionalities and SEI formation during Li intercalation, Carbon 92 (2015) 193–244, http://dx.doi.org/10.1016/j.carbon.2015.04.007.
[145] J. Yan, B.-J. Xia, Y.-C. Su, X.-Z. Zhou, et al., Phenomenologically modeling the formation and evolution of the solid electrolyte interface on the graphite electrode for lithium-ion batteries, Electrochim. Acta 53 (2008) 7069–7078, http://dx.doi.org/10.1016/j.electacta.2008.05.032.
[146] K.M. Abraham, Directions in secondary lithium battery research and development, Electrochem. Acta 38 (1993) 1233–1248, http://dx.doi.org/10.1016/0013-4686(93)80054-4.
[147] S.S. Zhang, K. Xu, T.R. Jow, EIS study on the formation of solid electrolyte interface in Li-ion battery, Electrochim. Acta 51 (8–9) (2006) 1636–1640, http://dx.doi.org/10.1016/j.electacta.2005.02.137.
[148] P. Ping, Q. Wang, J. Sun, X. Feng, et al., Effect of sulfites on the performance of LiBOB/γ-butyrolactone electrolytes, J. Power Sources 196 (2) (2011) 776–783, http://dx.doi.org/10.1016/j.jpowsour.2010.07.064.
[149] X. Cui, H. Zhang, S. Li, X. Li, et al., Electrochemical performances of a novel lithium bis(oxalate)borate-based electrolyte for lithium-ion batteries with LiFePO4 cathodes, Ionics 20 (6) (2014) 789–794, http://dx.doi.org/10.1007/s11581-013-1034-7.
[150] K. Tasaki, K. Kanda, T. Kobayashi, S. Nakamura, et al., Theoretical studies on the reductive decompositions of solvents and additives for lithium-ion batteries near lithium anodes, J. Electrochem. Soc. 153 (2006) A2192–A2197, http://dx.doi.org/10.1149/1.2354460.
[151] S. Flandroisa, B. Simon, Carbon materials for lithium-ion rechargeable batteries, Carbon 37 (1999) 165–180, http://dx.doi.org/10.1016/S0008-6223(98)00290-5.
[152] S.-H. Lee, H.-G. You, K.-S. Han, J. Kim, et al., A new approach to surface properties of solid electrolyte interphase on a graphite negative electrode, J. Power Sources 247 (2014) 307–313, http://dx.doi.org/10.1016/j.jpowsour.2013.08.105.
[153] S. Yoon, H. Kim, J.-J. Cho, Y.-K. Han, et al., Lactam derivatives as solid electrolyte interphase forming additives for a graphite anode of lithium-ion batteries, J. Power Sources 244 (2013) 711–715, http://dx.doi.org/10.1016/j.jpowsour.2012.11.115.
[154] H.M. Jung, S.-H. Park, J. Jeon, Y. Choi, et al., Fluoropropane sultone as an SEI-forming additive that outperforms vinylene carbonate, J. Mater. Chem. A 1 (2013) 11975–11981, http://dx.doi.org/10.1039/c3ta12580g.
[155] Y. Wang, S. Nakamura, M. Ue, P.B. Balbuena, Theoretical studies to understand surface chemistry on carbon anodes for lithium-ion batteries: reduction mechanisms of ethylene carbonate, J. Am. Chem. Soc. 123 (2001) 11708–11718, http://dx.doi.org/10.1021/ja0164529.
[156] Y. Wang, S. Nakamura, K. Tasaki, P.B. Balbuena, Theoretical studies to understand surface chemistry on carbon anodes for lithium-ion batteries: how does vinylene carbonate play its role as an electrolyte additive? J. Am. Chem. Soc. 124 (2002) 4408–4421, http://dx.doi.org/10.1021/ja017073i.
[157] R. Fong, Sacken Uy, J.R. Dahn, Studies of lithium intercalation into carbons using nonaqueous electrochemical cells, J. Electrochem. Soc. 137 (1990) 2009–2013, http://dx.doi.org/10.1149/1.2086855.
[158] I. Epelboin, M. Froment, M. Garreau, J. Thevenin, et al., Behavior of secondary lithium and aluminum-lithium electrode in propylene carbonate, J. Electrochem. Soc. 127 (1980) 2100–2104, http://dx.doi.org/10.1149/1.2129354.
[159] O. Crowther, A.C. West, Effect of electrolyte composition on lithium dendrite growth, J. Electrochem. Soc. 155 (2008) A806–A811, http://dx.doi.org/10.1149/1.2969424.
[160] M. Arakawa, S.-I. Tobishima, Y. Nemoto, M. Ichimura, et al., Lithium electrode cycleability and morphology dependence on current density, J. Power Sources 43–44 (1993) 27–35, http://dx.doi.org/10.1016/0378-7753(93)80099-B.
[161] K. Brandt, Historical development of secondary lithium batteries, Solid State Ion. 69 (1994) 173–183, http://dx.doi.org/10.1016/0167-2738(94)90408-1.
[162] T.D. Tran, J.H. Feikert, R.W. Pekala, Rate effect on lithium-ion graphite electrode performance, J. Appl. Electrochem. 26 (1996) 1161–1167, http://dx.doi.org/10.1007/BF00243741.
[163] S. Bhattacharya, A.R. Riahi, A.T. Alpas, Role of voltage scan rate on degradation of graphite electrodes electrochemically cycled vs. Li/Li+, MRS Proc. 1388 (2012) 1–6, http://dx.doi.org/10.1557/opl.2012.8.
[164] X. Zhang, R. Kostecki, T.J. Richardson, J.K. Pugh, et al., Electrochemical and infrared studies of the reduction of organic carbonates, J. Electrochem. Soc. 148 (12) (2001) A1341–A1345, http://dx.doi.org/10.1149/1.1415547.
[165] D. Aurbach, B. Markovsky, A. Shechter, Y. Ein-Eli, et al., A comparative study of synthetic graphite and Li electrodes in electrolyte solutions based on ethylene carbonate-dimethyl carbonate mixtures, J. Electrochem. Soc. 143 (1996) 3809–3820, http://dx.doi.org/10.1149/1.1837300.
[166] T. Eriksson, A.M. Andersson, A.G. Bishop, C. Gejke, et al., Surface analysis of LiMn[sub 2]O[sub 4] electrodes in carbonate-based electrolytes, J. Electrochem. Soc. 149 (1) (2002) A69–A78, http://dx.doi.org/10.1149/1.1426398.
[167] D. Aurbach, Review of selected electrode–solution interactions which determine the performance of Li and Li ion batteries, J. Power Sources 89 (2000) 206–218, http://dx.doi.org/10.1016/S0378-7753(00)00431-6.
[168] D. Aurbach, A. Zaban, Y. Ein-Eli, I. Weissman, et al., Recent studies on the correlation between surface chemistry, morphology, three-dimensional structures and performance of Li and Li-C intercalation anodes in several important electrolyte systems, J. Power Sources 68 (1997) 91–98, http://dx.doi.org/10.1016/S0378-7753(97)02575-5.
[169] T. Kawamura, A. Kimura, M. Egashira, S. Okada, et al., Thermal stability of alkyl carbonate mixed-solvent electrolytes for lithium ion cells, J. Power Sources 104 (2002) 260–264, http://dx.doi.org/10.1016/S0378-7753(01)00960-0.
[170] S.E. Sloop, J.K. Pugh, S. Wang, J.B. Kerr, et al., Chemical reactivity of PF[sub 5] and LiPF[sub 6] in ethylene carbonate/dimethyl carbonate solutions, Electrochem. Solid State Lett. 4 (4) (2001) A42–A44, http://dx.doi.org/10.1149/1.1353158.
[171] V.A. Agubra, J.W. Fergus, The formation and stability of the solid electrolyte interface on the graphite anode, J. Power Sources 268 (2014) 153–162, http://dx.doi.org/10.1016/j.jpowsour.2014.06.024.
[172] V.A. Agubra, J.W. Fergus, R. Fu, S.-y. Choe, Analysis of the deposit layer from electrolyte side reaction on the anode of the pouch type lithium ion polymer batteries: the effect of state of charge and charge rate, Electrochim. Acta 149 (2014) 1–10, http://dx.doi.org/10.1016/j.electacta.2014.10.076.
[173] V.A. Agubra, J.W. Fergus, R. Fu, S.-Y. Choe, Analysis of effects of the state of charge on the formation and growth of the deposit layer on graphite electrode of pouch type lithium ion polymer batteries, J. Power Sources 270 (2014) 213–220, http://dx.doi.org/10.1016/j.jpowsour.2014.07.126.
[174] M.M. Thackeray, A. Dekock, M.H. Rossouw, D. Liles, et al., Spinel electrodes from the Li-Mn-O system for rechargeable lithium battery applications, J. Electrochem. Soc. 139 (1992) 363–366, http://dx.doi.org/10.1149/1.2069222.
[175] A.K. Padhi, K.S. Nanjundaswamy, J.B. Goodenough, Phospho-olivines as positive-electrode materials for rechargeable lithium batteries, J. Electrochem. Soc. 144 (1997) 1188–1194, http://dx.doi.org/10.1149/1.1837571.
[176] S. Bhattacharya, A.R. Riahi, A.T. Alpas, Electrochemical cycling behaviour of lithium carbonate (Li2CO3) pre-treated graphite anodes – SEI formation and graphite damage mechanisms, Carbon 77 (2014) 99–112, http://dx.doi.org/10.1016/j.carbon.2014.05.011.
[177] M.E. Spahr, H. Wilhelm, F. Joho, J.-C. Panitz, et al., Purely hexagonal graphite and the influence of surface modifications on its electrochemical lithium insertion properties, J. Electrochem. Soc. 149 (8) (2002) A960–A966, http://dx.doi.org/10.1149/1.1486238.
[178] Y.-J. Han, J. Kim, J.-S. Yeo, J.C. An, et al., Coating of graphite anode with coal tar pitch as an effective precursor for enhancing the rate performance in Li-ion batteries: effects of composition and softening points of coal tar pitch, Carbon 94 (2015) 432–438, http://dx.doi.org/10.1016/j.carbon.2015.07.030.
[179] I. Kuribayashi, M. Yokoyama, M. Yamashita, Battery characteristics with various carbonaceous materials, J. Power Sources 54 (1995) 1–5, http://dx.doi.org/10.1016/0378-7753(94)02030-7.
[180] Y. Zhan, B. Zhang, L. Cao, X. Wu, et al., Iodine doped graphene as anode material for lithium ion battery, Carbon 94 (2015) 1–8, http://dx.doi.org/10.1016/j.carbon.2015.06.039.
[181] J.C. Ye, S. Charnvanichborikarn, M.A. Worsley, S.O. Kucheyev, et al., Enhanced electrochemical performance of ion-beam-treated 3D graphene aerogels for lithium ion batteries, Carbon 85 (2015) 269–278, http://dx.doi.org/10.1016/j.carbon.2014.12.097.
[182] K. Ushirogata, K. Sodeyama, Y. Okuno, Y. Tateyama, Additive effect on reductive decomposition and binding of carbonate-based solvent toward solid electrolyte interphase formation in lithium-ion battery, J. Am. Chem. Soc. 135 (32) (2013) 11967–11974, http://dx.doi.org/10.1021/ja405079s.
[183] K. Leung, S.B. Rempe, M.E. Foster, Y. Ma, et al., Modeling electrochemical decomposition of fluoroethylene carbonate on silicon anode surfaces in lithium ion batteries, J. Electrochem. Soc. 161 (3) (2013) A213–A221, http://dx.doi.org/10.1149/2.092401jes.
[184] K. Leung, Two-electron reduction of ethylene carbonate: a quantum chemistry re-examination of mechanisms, Chem. Phys. Lett. 568–569 (2013) 1–8, http://dx.doi.org/10.1016/j.cplett.2012.08.022.
[185] K. Leung, First-principles modeling of the initial stages of organic solvent decomposition on LixMn2O4(100) surfaces, J. Phys. Chem. C 116 (18) (2012) 9852–9861, http://dx.doi.org/10.1021/jp212415x.
[186] K. Leung, J. Budzien, Ab initio molecular dynamics simulations of the initial

stages of solid-electrolyte interphase formation on lithium ion battery graphitic anodes, Phys. Chem. Chem. Phys. 12 (2010) 6583–6586, http://dx.doi.org/10.1039/b925853a.
[187] R.J. Blint, Binding of ether and carbonyl oxygens to lithium ion, J. Electrochem. Soc. 142 (1995) 696–702, http://dx.doi.org/10.1149/1.2048519.
[188] M.D. Bhatt, M. Cho, K. Cho, Density functional theory calculations and ab initio molecular dynamics simulations for diffusion of Li+within liquid ethylene carbonate, Model. Simul. Mater. Sci. Eng. 20 (6) (2012) 065004, http://dx.doi.org/10.1088/0965-0393/20/6/065004.
[189] O. Borodin, G.V. Zhuang, P.N. Ross, K. Xu, Molecular dynamics simulations and experimental study of lithium ion transport in dilithium ethylene dicarbonate, J. Phys. Chem. C 117 (15) (2013) 7433–7444, http://dx.doi.org/10.1021/jp4000494.
[190] A. von Wald Cresce, O. Borodin, K. Xu, Correlating Li+ solvation sheath structure with interphasial chemistry on graphite, J. Phys. Chem. C 116 (50) (2012) 26111–26117, http://dx.doi.org/10.1021/jp303610t.
[191] O. Borodin, G.D. Smith, Quantum chemistry and molecular dynamics simulation study of dimethyl carbonate: ethylene carbonate electrolytes doped with LiPF6, J. Phys. Chem. B 113 (2009) 1763–1776, http://dx.doi.org/10.1021/jp809614h.
[192] Z. Wang, S.M. Selbach, T. Grande, Van der Waals density functional study of the energetics of alkali metal intercalation in graphite, RSC Adv. 4 (8) (2014) 3973–3983, http://dx.doi.org/10.1039/c3ra47187j.
[193] Z. Liu, J.Z. Liu, Y. Cheng, Z. Li, et al., Interlayer binding energy of graphite: a mesoscopic determination from deformation, Phys. Rev. B 85 (20) (2012), http://dx.doi.org/10.1103/PhysRevB.85.205418.
[194] R. Zacharia, H. Ulbricht, T. Hertel, Interlayer cohesive energy of graphite from thermal desorption of polyaromatic hydrocarbons, Phys. Rev. B 69 (15) (2004), http://dx.doi.org/10.1103/PhysRevB.69.155406.
[195] L.X. Benedict, N.G. Chopra, M.L. Cohen, A. Zettl, et al., Microscopic determination of the interlayer binding energy in graphite, Chem. Phys. Lett. 286 (1998) 490–496, http://dx.doi.org/10.1016/S0009-2614(97)01466-8.
[196] R. Jorn, R. Kumar, D.P. Abraham, G.A. Voth, Atomistic modeling of the electrode–electrolyte interface in li-ion energy storage systems: electrolyte structuring, J. Phys. Chem. C 117 (8) (2013) 3747–3761, http://dx.doi.org/10.1021/jp3102282.
[197] K. Omichi, G. Ramos-Sanchez, R. Rao, N. Pierce, et al., Origin of excess irreversible capacity in lithium-ion batteries based on carbon nanostructures, J. Electrochem. Soc. 162 (10) (2015) A2106–A2115, http://dx.doi.org/10.1149/2.0591510jes.
[198] K. Ushirogata, K. Sodeyama, Z. Futera, Y. Tateyama, et al., Near-shore aggregation mechanism of electrolyte decomposition products to explain solid electrolyte interphase formation, J. Electrochem. Soc. 162 (14) (2015) A2670–A2678, http://dx.doi.org/10.1149/2.0301514jes.
[199] K. Tasaki, A. Goldberg, M. Winter, On the difference in cycling behaviors of lithium-ion battery cell between the ethylene carbonate- and propylene carbonate-based electrolytes, Electrochim. Acta 56 (28) (2011) 10424–10435, http://dx.doi.org/10.1016/j.electacta.2011.05.112.
[200] K. Persson, Y. Hinuma, Y.S. Meng, A. Van der Ven, et al., Thermodynamic and kinetic properties of the Li-graphite system from first-principles calculations, Phys. Rev. B 82 (12) (2010), http://dx.doi.org/10.1103/PhysRevB.82.125416.
[201] Y. Qi, H. Guo, L.G. Hector, A. Timmons, Threefold increase in the young's modulus of graphite negative electrode during lithium intercalation, J. Electrochem. Soc. 157 (5) (2010) A558, http://dx.doi.org/10.1149/1.3327913.
[202] K.R. Kganyago, P.E. Ngoepe, Structural and electronic properties of lithium intercalated graphiteLiC6, Phys. Rev. B 68 (20) (2003), http://dx.doi.org/10.1103/PhysRevB.68.205111.
[203] O. Borodin, M. Olguin, C. Spear, K. Leiter, et al., Challenges with quantum chemistry-based screening of electrochemical stability of lithium battery electrolytes, ECS Trans. 69 (1) (2015) 113–123, http://dx.doi.org/10.1149/06901.0113ecst.
[204] G. Gourdin, D. Zheng, D. Qu, Adaption of kinetics to solid electrolyte interphase layer formation and application to electrolyte-soluble reaction products, J. Power Sources 299 (2015) 451–459, http://dx.doi.org/10.1016/j.jpowsour.2015.08.072.
[205] G. Gourdin, J. Collins, D. Zheng, M. Foster, et al., Spectroscopic compositional analysis of electrolyte during initial SEI layer formation, J. Phys. Chem. C 118 (31) (2014) 17383–17394, http://dx.doi.org/10.1021/jp504181b.
[206] D. Aurbach, B. Markovsky, M.D. Levi, E. Levi, et al., New insights into the interactions between electrode materials and electrolyte solutions for advanced nonaqueous batteries, J. Power Sources 81–82 (1999) 95–111.
[207] X. Teng, C. Zhan, Y. Bai, L. Ma, et al., In situ analysis of gas generation in lithium-ion batteries with different carbonate-based electrolytes, ACS Appl. Mater. Interfaces 7 (41) (2015) 22751–22755, http://dx.doi.org/10.1021/acsami.5b08399.
[208] L. Xing, W. Li, C. Wang, F. Gu, et al., Theoretical investigations on oxidative stability of solvents and oxidative decomposition mechanism of ethylene carbonate for lithium ion battery use, J. Phys. Chem. B 113 (2009) 16596–16602, http://dx.doi.org/10.1021/jp9074064.
[209] B. Liang, Y. Liu, Y. Xu, Silicon-based materials as high capacity anodes for next generation lithium ion batteries, J. Power Sources 267 (2014) 469–490, http://dx.doi.org/10.1016/j.jpowsour.2014.05.096.
[210] X. Su, Q. Wu, J. Li, X. Xiao, et al., Silicon-based nanomaterials for lithium-ion batteries: a review, Adv. Energy Mater. 4 (1) (2014) 1–23, http://dx.doi.org/10.1002/aenm.201300882.
[211] S. Goriparti, E. Miele, F. De Angelis, E. Di Fabrizio, et al., Review on recent progress of nanostructured anode materials for Li-ion batteries, J. Power Sources 257 (2014) 421–443, http://dx.doi.org/10.1016/j.jpowsour.2013.11.103.
[212] M. Li, J. Gu, X. Feng, H. He, et al., Amorphous-silicon@silicon oxide/chromium/carbon as an anode for lithium-ion batteries with excellent cyclic stability, Electrochim. Acta 164 (2015) 163–170, http://dx.doi.org/10.1016/j.electacta.2015.02.224.
[213] Y. Xu, Y. Zhu, Y. Liu, C. Wang, Electrochemical performance of porous carbon/tin composite anodes for sodium-ion and lithium-ion batteries, Adv. Energy Mater. 3 (1) (2013) 128–133, http://dx.doi.org/10.1002/aenm.201200346.
[214] K.K.D. Ehinon, S. Naille, R. Dedryve're, P.-E. Lippens, et al., Ni3Sn4 electrodes for Li-ion batteries- Li–Sn alloying process and electrode electrolyte interface phenomena, Chem. Mater. 20 (2008) 5388–5398, http://dx.doi.org/10.1021/cm8006099.
[215] X.J. Zhu, Z.P. Guo, P. Zhang, G.D. Du, et al., Highly porous reticular tin–cobalt oxide composite thin film anodes for lithium ion batteries, J. Mater. Chem. 19 (44) (2009) 8360–8365, http://dx.doi.org/10.1039/b913993a.
[216] M. Mouyane, L. Aldon, M. Womes, B. Ducourant, et al., Tin dispersed in an oxide matrix as negative electrode material for Li-ion batteries, J. Power Sources 189 (1) (2009) 818–822, http://dx.doi.org/10.1016/j.jpowsour.2008.07.047.
[217] L. Ji, Z. Tan, T. Kuykendall, E.J. An, et al., Multilayer nanoassembly of Sn-nanopillar arrays sandwiched between graphene layers for high-capacity lithium storage, Energy Environ. Sci. 4 (9) (2011) 3611–3616, http://dx.doi.org/10.1039/c1ee01592c.
[218] G. Wang, B. Wang, X. Wang, J. Park, et al., Sn/graphene nanocomposite with 3D architecture for enhanced reversible lithium storage in lithium ion batteries, J. Mater. Chem. 19 (44) (2009) 8378–8384, http://dx.doi.org/10.1039/b914650d.
[219] R. Hu, H. Liu, M. Zeng, H. Wang, et al., Core/shell and multi-scale structures enhance the anode performance of a Sn–C–Ni composite thin film in a lithium ion battery, J. Mater. Chem. 21 (12) (2011) 4629–4635, http://dx.doi.org/10.1039/c0jm04173d.
[220] M. Mouyane, J.M. Ruiz, M. Artus, S. Cassaignon, et al., Carbothermal synthesis of Sn-based composites as negative electrode for lithium-ion batteries, J. Power Sources 196 (16) (2011) 6863–6869, http://dx.doi.org/10.1016/j.jpowsour.2010.09.001.
[221] N. Li, H. Song, H. Cui, C. Wang, Sn@graphene grown on vertically aligned graphene for high-capacity, high-rate, and long-life lithium storage, Nano Energy 3 (2014) 102–112, http://dx.doi.org/10.1016/j.nanoen.2013.10.014.
[222] W. Li, R. Yang, J. Zheng, X. Li, Tandem plasma reactions for Sn/C composites with tunable structure and high reversible lithium storage capacity, Nano Energy 2 (6) (2013) 1314–1321, http://dx.doi.org/10.1016/j.nanoen.2013.06.012.
[223] Y. Xu, Q. Liu, Y. Zhu, Y. Liu, et al., Uniform nano-Sn/C composite anodes for lithium ion batteries, Nano Lett. 13 (2) (2013) 470–474, http://dx.doi.org/10.1021/nl303823k.
[224] Q. Yun, X. Qin, W. Lv, Y.-B. He, et al., “Concrete” inspired construction of a silicon/carbon hybrid electrode for high performance lithium ion battery, Carbon 93 (2015) 59–67, http://dx.doi.org/10.1016/j.carbon.2015.05.032.
[225] J. Wu, X. Qin, H. Zhang, Y.-B. He, et al., Multilayered silicon embedded porous carbon/graphene hybrid film as a high performance anode, Carbon 84 (2015) 434–443, http://dx.doi.org/10.1016/j.carbon.2014.12.036.
[226] X.-H. Li, Y.-B. He, C. Miao, X. Qin, et al., Carbon coated porous tin peroxide/carbon composite electrode for lithium-ion batteries with excellent electrochemical properties, Carbon 81 (2015) 739–747, http://dx.doi.org/10.1016/j.carbon.2014.10.016.
[227] F. Zhang, X. Yang, Y. Xie, N. Yi, et al., Pyrolytic carbon-coated Si nanoparticles on elastic graphene framework as anode materials for high-performance lithium-ion batteries, Carbon 82 (2015) 161–167, http://dx.doi.org/10.1016/j.carbon.2014.10.046.
[228] M. Joe, Y.-K. Han, K.-R. Lee, H. Mizuseki, et al., An ideal polymeric C60 coating on a Si electrode for durable Li-ion batteries, Carbon 77 (2014) 1140–1147, http://dx.doi.org/10.1016/j.carbon.2014.06.049.
[229] A.Y. Kim, J.S. Kim, C. Hudaya, D. Xiao, et al., An elastic carbon layer on echeveria-inspired SnO2 anode for long-cycle and high-rate lithium ion batteries, Carbon 94 (2015) 539–547, http://dx.doi.org/10.1016/j.carbon.2015.07.041.
[230] C. Ma, C. Ma, J. Wang, H. Wang, et al., Exfoliated graphite as a flexible and conductive support for Si-based Li-ion battery anodes, Carbon 72 (2014) 38–46, http://dx.doi.org/10.1016/j.carbon.2014.01.027.
[231] Y. Yu, L. Gu, X. Lang, C. Zhu, et al., Li storage in 3D nanoporous Au-supported nanocrystalline tin, Adv. Mater. 23 (21) (2011) 2443–2447, http://dx.doi.org/10.1002/adma.201004331.
[232] B. Luo, B. Wang, X. Li, Y. Jia, et al., Graphene-confined Sn nanosheets with enhanced lithium storage capability, Adv. Mater. 24 (26) (2012) 3538–3543, http://dx.doi.org/10.1002/adma.201201173.
[233] X. Zhou, L.J. Wan, Y.G. Guo, Binding SnO2 nanocrystals in nitrogen-doped graphene sheets as anode materials for lithium-ion batteries, Adv. Mater. 25 (15) (2013) 2152–2157, http://dx.doi.org/10.1002/adma.201300071.
[234] Y. Wang, M. Wu, Z. Jiao, J.Y. Lee, Sn@CNT and Sn@C@CNT nanostructures for superior reversible lithium ion storage, Chem. Mater. 21 (14) (2009)

3210–3215, http://dx.doi.org/10.1021/cm900702d.
[235] F. Nobili, I. Meschini, M. Mancini, R. Tossici, et al., High-performance Sn@carbon nanocomposite anode for lithium-ion batteries: lithium storage processes characterization and low-temperature behavior, Electrochim. Acta 107 (2013) 85–92, http://dx.doi.org/10.1016/j.electacta.2013.05.150.
[236] L. Zhang, H.B. Wu, B. Liu, X.W. Lou, Formation of porous SnO2 microboxes via selective leaching for highly reversible lithium storage, Energy Environ. Sci. 7 (3) (2014) 1013–1017, http://dx.doi.org/10.1039/c3ee43305f.
[237] Q. Tian, Z. Zhang, L. Yang, S.-i. Hirano, Three-dimensional wire-in-tube hybrids of tin dioxide and nitrogen-doped carbon for lithium ion battery applications, Carbon 93 (2015) 887–895, http://dx.doi.org/10.1016/j.carbon.2015.06.010.
[238] L. Sun, X. Wang, R.A. Susantyoko, Q. Zhang, High performance binder-free Sn coated carbon nanotube array anode, Carbon 82 (2015) 282–287, http://dx.doi.org/10.1016/j.carbon.2014.10.072.
[239] F. Yao, B. Li, K. So, J. Chang, et al., A strategy to overcome the limits of carbon-based materials as lithium-ion battery anodes, Carbon 79 (2014) 563–571, http://dx.doi.org/10.1016/j.carbon.2014.08.017.
[240] M. Ihsan, H. Wang, S.R. Majid, J. Yang, et al., MoO2/Mo2C/C spheres as anode materials for lithium ion batteries, Carbon 96 (2016) 1200–1207, http://dx.doi.org/10.1016/j.carbon.2015.10.076.
[241] X. Xu, H. Tan, K. Xi, S. Ding, et al., Bamboo-like amorphous carbon nanotubes clad in ultrathin nickel oxide nanosheets for lithium-ion battery electrodes with long cycle life, Carbon 84 (2015) 491–499, http://dx.doi.org/10.1016/j.carbon.2014.12.040.
[242] H. Liu, Z. Li, Y. Liang, R. Fu, et al., Facile synthesis of MnO multi-core@nitrogen-doped carbon shell nanoparticles for high performance lithium-ion battery anodes, Carbon 84 (2015) 419–425, http://dx.doi.org/10.1016/j.carbon.2014.12.032.
[243] R.A. Susantyoko, X. Wang, Y. Fan, Q. Xiao, et al., Stable cyclic performance of nickel oxide–carbon composite anode for lithium-ion batteries, Thin Solid Films 558 (2014) 356–364, http://dx.doi.org/10.1016/j.tsf.2014.01.087.
[244] R.A. Susantyoko, X. Wang, Q. Xiao, E. Fitzgerald, et al., Sputtered nickel oxide on vertically-aligned multiwall carbon nanotube arrays for lithium-ion batteries, Carbon 68 (2014) 619–627, http://dx.doi.org/10.1016/j.carbon.2013.11.041.
[245] C. Kang, R. Baskaran, J. Hwang, B.-C. Ku, et al., Large scale patternable 3-dimensional carbon nanotube–graphene structure for flexible Li-ion battery, Carbon 68 (2014) 493–500, http://dx.doi.org/10.1016/j.carbon.2013.11.026.
[246] B. Rangasamy, J.Y. Hwang, W. Choi, Multi layered Si–CuO quantum dots wrapped by graphene for high-performance anode material in lithium-ion battery, Carbon 77 (2014) 1065–1072, http://dx.doi.org/10.1016/j.carbon.2014.06.022.
[247] J. Zhang, Z. Xie, W. Li, S. Dong, et al., High-capacity graphene oxide/graphite/carbon nanotube composites for use in Li-ion battery anodes, Carbon 74 (2014) 153–162, http://dx.doi.org/10.1016/j.carbon.2014.03.017.
[248] D. Wang, J. Yang, J. Liu, X. Li, et al., Atomic layer deposited coatings to significantly stabilize anodes for Li ion batteries: effects of coating thickness and the size of anode particles, J. Mater. Chem. A 2 (7) (2014) 2306–2312, http://dx.doi.org/10.1039/c3ta13677a.
[249] M. Yu, A. Wang, Y. Wang, C. Li, et al., An alumina stabilized ZnO-graphene anode for lithium ion batteries via atomic layer deposition, Nanoscale 6 (19) (2014) 11419–11424, http://dx.doi.org/10.1039/c4nr02576h.
[250] G. Zheng, S.W. Lee, Z. Liang, H.W. Lee, et al., Interconnected hollow carbon nanospheres for stable lithium metal anodes, Nat. Nanotechnol. 9 (8) (2014) 618–623, http://dx.doi.org/10.1038/nnano.2014.152.
[251] R. Bouchet, A stable lithium metal interface, Nat. Nanotechnol. 9 (2014) 572–573, http://dx.doi.org/10.1038/nnano.2014.165.
[252] I.A. Shkrob, T.W. Marin, Y. Zhu, D.P. Abraham, Why Bis(fluorosulfonyl)imide is a “magic anion” for electrochemistry, J. Phys. Chem. C 118 (34) (2014) 19661–19671, http://dx.doi.org/10.1021/jp506567p.
[253] V. Etacheri, O. Haik, Y. Goffer, G.A. Roberts, et al., Effect of fluoroethylene carbonate (FEC) on the performance and surface chemistry of Si-nanowire Li-ion battery anodes, Langmuir ACS J. Surf. Colloids 28 (1) (2012) 965–976, http://dx.doi.org/10.1021/la203712s.
[254] N.-S. Choi, K.H. Yew, K.Y. Lee, M. Sung, et al., Effect of fluoroethylene carbonate additive on interfacial properties of silicon thin-film electrode, J. Power Sources 161 (2) (2006) 1254–1259, http://dx.doi.org/10.1016/j.jpowsour.2006.05.049.
[255] K. Eom, J. Jung, J.T. Lee, V. Lair, et al., Improved stability of nano-Sn electrode with high-quality nano-SEI formation for lithium ion battery, Nano Energy 12 (2015) 314–321, http://dx.doi.org/10.1016/j.nanoen.2014.12.041.
[256] I.A. Shkrob, J.F. Wishart, D.P. Abraham, What makes fluoroethylene carbonate different? J. Phys. Chem. C 119 (27) (2015) 14954–14964, http://dx.doi.org/10.1021/acs.jpcc.5b03591.
[257] J.M. Martinez de la Hoz, F.A. Soto, P.B. Balbuena, Effect of the electrolyte composition on sei reactions at Si anodes of Li-ion batteries, J. Phys. Chem. C 119 (13) (2015) 7060–7068, http://dx.doi.org/10.1021/acs.jpcc.5b01228.
[258] Y. Zhu, M.D. Casselman, Y. Li, A. Wei, et al., Perfluoroalkyl-substituted ethylene carbonates: novel electrolyte additives for high-voltage lithium-ion batteries, J. Power Sources 246 (2014) 184–191, http://dx.doi.org/10.1016/j.jpowsour.2013.07.070.
[259] Y. Zhu, Y. Li, M. Bettge, D.P. Abraham, Electrolyte additive combinations that enhance performance of high-capacity Li1.2Ni0.15Mn0.55Co0.1O2–graphite cells, Electrochim. Acta 110 (2013) 191–199, http://dx.doi.org/10.1016/j.electacta.2013.03.102.
[260] R. Wagner, S. Brox, J. Kasnatscheew, D.R. Gallus, et al., Vinyl sulfones as SEI-forming additives in propylene carbonate based electrolytes for lithium-ion batteries, Electrochem. Commun. 40 (2014) 80–83, http://dx.doi.org/10.1016/j.elecom.2014.01.004.
[261] F. Chrétien, J. Jones, C. Damas, D. Lemordant, et al., Impact of solid electrolyte interphase lithium salts on cycling ability of Li-ion battery: beneficial effect of glymes additives, J. Power Sources 248 (2014) 969–977, http://dx.doi.org/10.1016/j.jpowsour.2013.09.092.